CHARACTERIZATION OF SELECTED SURFACE TREATMENTS FOR CONCRETE PAVEMENT

A Thesis

by

CARL NAZIH ABOU SLEIMAN

Submitted to the Office of Graduate and Professional Studies of
Texas A&M University
in partial fulfillment of the requirements for the degree of

MASTER OF SCIENCE

Chair of Committee,	Dan G. Zollinger
Co-Chair of Committee,	Zachary Grasley
Committee Members,	Ankit Srivastava
Head of Department,	Robin Autenrieth

August 2019

Major Subject: Civil Engineering

ABSTRACT

For a concrete pavement, the permeation properties for the surface have a crucial influence on its durability. Current practices assess the resistance of the surface to abrasion and freeze/thaw cycles based primarily on the compression strength of the concrete. A prominent way to enhance the durability of concrete is by use of surface treatments to reduce water and chloride penetration. In other words, surface treatments partake in protecting concrete surfaces from the ingress of deleterious substances such as salt, organic impurities and dust. The objective of this thesis is to investigate the efficiency of organic and inorganic surface treatments regarding abrasion, freeze/thaw damage, water and chloride penetration. ASTM standards were modified to abbreviate the testing and assess the efficiency of different products. Based on the tests performed, organic surface treatments remarkably increased the resistance of concrete subjected to freeze/thaw cycles by reducing the water intake compared to the inorganic ones. Similar results were observed regarding the chloride penetration test leading to an improvement in durability. The abrasion resistance of a concrete surface can be improved using inorganic surface treatments based on lithium and silicon. A model was proposed to relate the abrasion efficiency as a function of load cycles of a treated surface to represent the longevity of a concrete pavement. Based on the abrasion coefficient and the texture wavelength which is a measurement of the quality of the surface of the pavement, it is shown that the life cycle under abrasion of a concrete pavement can be calibrated. As part of the laboratory testing program, the untreated concrete specimens were used as the control. Results from the

abrasion and freeze/thaw testing of treated specimens indicated a lower level of cumulative damage, which confirmed the benefit of using such products relative to the extension of the service life of a concrete pavement surface. The results of modeling indicated an increase of 14% of the ultimate load application to failure for the treated specimens, which indicates an increase in longevity of the pavement.

DEDICATION

To my mother Michele Saliba Abou Sleiman, my father Nazih Abou Sleiman, my brother and two sisters Leon, Sacha and Gaelle.

If it wasn't hard, everyone would do it – Tom Hanks

ACKNOWLEDGEMENTS

Foremost, I would like to express my gratitude to my supervisor, Dr. Dan Zollinger, for the useful comments, remarks and engagement through the learning process of this master thesis. His encouragement since the first day of this journey led me to write a journal paper published in the *Transportation Research Record* after just three months of research. Thanks to my committee members, Dr. Srivastava and Dr. Grasley, for their support throughout the course of this research. Thank you Dr. Grasley for making me fall in love with the "concrete" material when I first took this class in Fall 2017.

I also owe many thanks to Dr. Anol Mukhopadhyay for his guidance in the analysis and his invaluable insight for this research. My sincere thanks also goes to Dr. Xijun Shi, Dr. Kai-Wei Liu and Dr. Pravat Karki for the help provided during the testing period. I also sincerely value my friends from the Zachry Department of Civil Engineering at Texas A&M University for their continued assistance and encouragement.

This work could not have been possible without the support from several facilities at Texas A&M University. The Center for Infrastructure Renewal gave me the opportunity to expand my laboratory work and research using the latest technologies. The Texas A&M Transportation Institute along with TxDOT provided me with the adequate equipment for my investigations. The Materials Lab at Zachry Department of Civil Engineering allowed me to perform several tests. I appreciate all the assistance provided by Rick Canatella, Ross Taylor, Ethan Karnei, Tony Barbosa, and Dave Dillon.

Finally, I am extremely thankful for all the love, support, and patience from my family. This thesis is dedicated to my family.

CONTRIBUTORS AND FUNDING SOURCES

Faculty committee recognition

This work was supervised by the committee consisting of Dr. Dan Zollinger (Advisor), Dr. Zachary Grasley (co-advisor) of the Zachry Department of Civil Engineering and Dr. Ankit Srivastava of the Materials Science & Engineering Department.

Student/Advisor contributions

All work for this dissertation was completed by the student, under the advisement of Dr. Dan Zollinger of the Zachry Department of Civil Engineering.

Funding sources

This work was made possible by Convergent Concrete Technologies LLC under the research project number 610271-00001. The contents of this work are solely the responsibility of the author and do not necessarily represent the official views of the sponsors.

TABLE OF CONTENTS

Page

LIST OF FIGURES

Page

LIST OF TABLES

Page

CHAPTER I

INTRODUCTION

Around the world, concrete is the most used material in civil engineering projects; more precisely concrete is the 2nd most consumed element in the world after water. In the United States, the concrete industry alone is worth over $35 billion. The reason why concrete is used in such massive quantities is purely because it is an extraordinary good building material; not just for rudimentary road construction but also for outstanding projects. For instance, in Dubai, the construction of Burj Khalifa used almost 239 million pounds of concrete, for the Grand Coulee Dam in Washington State, 48 billion pounds of concrete were utilized between 1933 and 1942. Due to the massive progress made in concrete technology in the past few decades, many applications have emerged. Compared to other engineered cementitious materials used on the construction field, the production cost of cement concrete is extremely low. Concrete gains its strength at ambient room temperature and can be optimized using admixtures. It has the ability to be cast in place, it is high temperature resistant and its maintenance cost can be almost negligible. On the contrary, concrete is brittle, has low tensile strength and faces durability issues.

The concrete material has been also used in the transportation field and more specifically in pavement design and materials area.

The first concrete pavement in the world was built in Inverness, Scotland in 1879 followed by the first U.S. concrete pavement constructed in Bellefontaine, Ohio in 1893. At first, concrete mixes were dry-batched, dumped into trucks and mixed on grade in fixed

forms. Traveling mixers evolved to provide a better uniform dry-batched concrete mixes. The AASHTO Road Test was conceived to study the performance of pavement structures under actual traffic at a known magnitude and frequency. Although many efforts were put into account to improve the quality of concrete pavements, rigid roads face numerous durability problems regarding the deterioration of the top surface and its effect on road safety, fuel consumption, tire wear and many others.

In order to improve the quality of concrete pavements against surface wear, many industries manufactured numerous products known as surface treatments that can be applied on a concrete surface. According to the manufacture's specifications, the product can reduce water penetration and improve the resistance to wear due to tires and freeze/thaw cycles.

Depending on its properties, the surface treatment shows some benefits that can be depicted through laboratory testing. In the following study, many surface treatments applied on concrete specimens were studied regarding their efficiency to improve wear caused by traffic and resistance to freeze/thaw damage by adopting destructive tests. Moreover, a variety of laboratory tests were conducted to study the effectiveness of these surface treatments regarding the porosity change of the surface and its effect on abrasion and freeze/thaw damage.

The testing program was to serve as a general overview of concrete durability. All tests were performed according to the ASTM standards even though some modifications were made to suit the purposes of the test program.

CHAPTER II

LITERATURE REVIEW[1]

Concrete is a composite material consisting of particles glued together with a cementing binder. Portland Cement Concrete (PCC) utilizes the Portland Cement as the binder agent. The mixture consists then of Portland Cement, water, aggregates (fine and coarse), mineral and chemical admixtures and finally air. Concrete has many advantages; it has the ability to be cast, it is durable, fire resistant, energy efficient, etc., but also has some disadvantages regarding its low tensile strength and low ductility, its volume instability and low strength-to-weight ratio (Mindess, Young, & Darwin, 2002)

The hydration process of Portland Cement explains many aspects regarding the physical behavior of the concrete. The main two hydration products of the cement are the Calcium-Silicate-Hydrate (CSH) and the Calcium Hydroxide (CH). In the mixture, CSH has a very complex microstructure due to its amorphous character, compositional variability and poorly resolved morphology. This product provides important cohesive force but is intrinsically weak because of its connected micro-porosity. On the other side, CH occupies approximately about 15% of the total volume of a normal Portland Cement paste. Calcium Hydroxide is a well-crystallized material with a definite stoichiometry. It

[1] Part of the contents in this chapter is reprinted with permission from:
An approach to characterize the wearability of concrete pavement surface treatments, by Abou Sleiman C., Shi X., and Zollinger D., Transportation Research Record: Journal of the Transportation Research Board, 2019. DOI: https://doi.org/10.1177/0361198118821668.

contributes to the durability of the concrete by reducing the porosity. By blocking the capillary pores, the calcium hydroxide reduces the permeability.

Understanding the chemistry of the different components of the concrete matrix will permit to improve its numerous properties to meet the challenge of the future.

1. Durability issue

The durability of a concrete pavement surface and its material wearability or resistance over time while exposed to traffic loading and environmental damaging effects has been a concern for many years. The abrasion life of a concrete pavement surface is likely a function of both repeated tire loading and the number of freeze/thaw cycles in the presence of deicer chemicals.

Wear cycles occur on concrete road surfaces due to tire loadings mainly from heavy trucks. The impact-cutting type of wear added to the abrasion action exacerbate the deterioration of the pavement. A significant source of wear is due to tire chains and studded snow tires that are mainly used in cold regions to increase the grip between the tires and the pavement that cause significant damage (ACI.2R-01, 2001). In fact, the dynamic impact of the small tungsten carbide tip of the tire studs repeatedly applies a shearing stress to the pavement surface under the rolling action of the tire. Studies showed that ruts from ¼ to ½ in (6 to 12 mm) deep can appear in just a single winter in regions where usually 30% of passenger cars are equipped with studded tires (ACI.2R-01, 2001) (Smith & Schonfeld, 1970-1978). This repeated action rapidly deteriorates the surface of the pavement, potentially causing roads safety issues. At one point, some effort was aimed at developing more wear-resistant types of concrete overlays such as using polymer-

cement and polymer-fly ash concretes (Keyser, 1971). No affordable concrete surface has been yet developed (ACI.2R-01, 2001). Since the abrasion occurs at the surface, the quality and strength of the cement paste is one of the main factors. One aspect of quality is the amount of calcium hydroxide in the hardened paste, which is directly related to the water-cementitious ratio (w/cm) used in the concrete (Scott & Safiuddin, 2015). This hydration product tends to be soft and erodible, often leading to microscopic pits in the surface of the concrete. Laboratory testing of the abrasion resistance of the concrete shows it to depend upon the paste hardness, the type of coarse aggregates and the strength of aggregate/paste bond (Scott & Safiuddin, 2015).

Freeze/thaw resistance is also influenced by the water-cement ratio as it dictates the amount of capillary-sized and large pores at the surface. These include gel pores, capillary pores and air voids (Harnik, Meier, & Rosli, 1980). Typically, concrete with a low permeability (i.e. mainly gel-sized and capillary-sized pores) is able to resist freeze/thaw cycles better than a concrete with a greater w/cm. With curing, permeability of the concrete decreases due to the hydration process of the cement and a reduction in capillary porosity. Other factors affecting freeze/thaw resistance are related to: the type of aggregates, the use of air-entrained admixtures and even the finishing method of the fresh concrete. During the freezing cycle, the water entrapped in the pores solidifies and turns into ice. This phenomenon expands the water by 9% and creates significant tensile stress (Yousif, 2015). Scaling due to several freeze/thaw cycles refers to a local flaking of a finished surface. This damage or scaling resistance is distinguished by the fracturing of

mortar, which leads to a direct exposure of the concrete to moisture penetration as well as aggressive salts (Jana, 2007).

Worldwide, the use of deicer chemicals has been employed in order to improve a roadways safety. The effect of a deicer on ice is related to the physical bonds formed between the solute which is the deicer and the solvent which is the water. Literature showed that the scaling at the surface is intensified in the presence of deicers used for pavement maintenance in winter, which is commonly known as salt frost deterioration (J. Marchand, 1994). The combined effect of freeze/thaw cycles and deicer chemicals on scaling potential is greater than when a concrete surface is exposed to freezing alone (Harnik, Meier, & Rosli, 1980). The use of deicer chemicals can increase the scaling damage at the surface as moisture tends to move towards zones with higher salt concentrations via osmosis and accelerates consequently the deterioration of concrete durability (Dang, et al., 2014). Indeed, the aqueous solution at the surface causes expansive forces inside the concrete microstructure and adds to the normal hydraulic pressure.

2. Assessment of the distresses

a) Abrasion models

Several studies resulted in different models of abrasive wear of concrete. E. Horszczaruk (Horszczaruk, 2004) presented a theoretical model based on results from abrasion-testing of concrete hydraulic structures due to the movement of rubble transported by water. The model was based on mechanisms associated with a concrete surface being exposed to the flow of an aggregate and water mixture. The study showed

that the mass loss in abraded concrete can be expressed as function of work by the abrasive aggregate/water mix and a parameter related to the resistance of the concrete.

Another study that extends the theoretical model developed by E. Horszczaruk expresses the material loss as a function of the abrasion effect caused by a rolling wheel and the total abrasion time, in addition to the composition of the concrete (Garcia, Castro-Fresno, Polanco, & Thomas, 2012). The model is based on Maxwell and Boltzmann distribution law to predict the volume of abraded pavement material in probabilistic terms. In addition to the applied force, the model incorporated the friction coefficient between the concrete and the wheel to characterize the abrasion resistance. Knowing these model parameters such as friction coefficient and the traffic configuration such as the weight of the vehicle on the pavement, a prediction of the concrete pavement service life can be obtained (Garcia, Castro-Fresno, Polanco, & Thomas, 2012).

An aspect of the modeling introduced in this thesis relates a micro-component of unevenness of a roadway surface that is generally expressed in terms of texture. Texture is not only an important impact regarding many aspects of road safety and comfort but also friction, smoothness, rolling resistance and tire wear (Cossale, Elliott, & Widyatmoko, 2013). The pavement texture is characterized by texture wavelength, ranging from microscopic (sub-millimeter) to long (several centimeters). The categories for texture wavelengths include megatexture (50 to 500 mm), macrotexture (0.5 to 50 mm), and microtexture (< 0.5 mm). The macrotexture is a function of the method of finishing used in the construction of the pavement surface. Microtexture is actually a

material's property dependent upon the fine particles in the concrete mix. Usually, the texture wavelength is measured using laser-based profilometry.

b) Freeze/thaw cycles

Freeze/thaw damage in concrete is a difficult phenomenon that has been studied for decades. Little in the literature has shown an accurate assessment of freeze/thaw damage on concrete surfaces; this assessment has been usually evaluated according to the ASTM C672 and ASTM C 666 following a visual grading system and not intended to give a quantitative measurement of the length of service of a concrete structure (Figure 1).

Rating	Condition of Surface
0	no scaling
1	very slight scaling (3 mm [⅛ in.] depth, max, no coarse aggregate visible)
2	slight to moderate scaling
3	moderate scaling (some coarse aggregate visible)
4	moderate to severe scaling
5	severe scaling (coarse aggregate visible over entire surface)

Figure 1: Visual rating for assessing Freeze/thaw damage (ASTM C 672, 2012)

The test method described in the ASTM C 672 (ASTM C 672, 2012) covers the determination of the resistance to scaling or flaking of the mortar of a horizontal concrete surface exposed to freeze/thaw cycles in the presence of deicing chemicals. This standard asserts that the method is *"intended for use in evaluating this surface resistance qualitatively by visual examination"*.

A visual assessment is a subjective way of evaluation, especially to compare the effectiveness of different surface treatments regarding frost damage. As a result, a quantitative measurement of the evolution of damage as a function of cycles cannot be

determined. A study done by Liu et al (Liu & Hansen, 2016) showed the effect of silane application on concrete surface exposed to freeze/thaw cycles. The mass loss was measured by weighing the specimen and determine its evolution as a function of cycles. No mathematical equation was present to predict this evolution according to the collected data. In addition, a regression analysis could have been made to determine the efficiency of the surface treatment regarding the different phases of freeze/thaw cycles.

3. Concrete surface treatments

The use of different surface treatments to protect the concrete surface from abrasion due to tire and freeze/thaw cycles in the presence of deicer chemicals has been widely elaborated (Pan, Shi, Shi, Ling, & Li, 2017). It is an economical way to protect the surface compared with other methods, such as decreasing the water to cement ratio or adding admixtures. It is widely acknowledged that a surface treatment has little effect on the strength of the concrete since it cannot improve the porosity and quality of the whole concrete matrix but only at the surface. The penetration depth of this chemical is often a few millimeters or even less (Pan, Shi, Shi, Ling, & Li, 2017).

The different types of surface treatments are classified according to the chemical composition of their active agents: Inorganic and organic treatments. Organic surface treatments are commonly used for their protective action on concrete surfaces although their application indicated some disadvantages regarding chloride ion penetration and long-life performance. Silane, an organic surface treatment, showed a good performance in reducing water penetration by making the surface hydrophobic but its capacity to stand wear is significantly low or non-existent. The hydrophobicity of a material designates its

capability to repulse water which depends on the surface geometry and chemical composition (Liu, Chen, & Xin, 2006). In addition, as a designation of the degree of hydrophobicity, the contact angle between a drop water or any liquid and the surface is usually pointed out. Hydrophobicity is indicated by a contact angle greater than 90˚; as this angle decreases (less than 90˚), the surface has the tendency to absorb water as shown in figure 2 (I. Flores-Vivian, 2013).

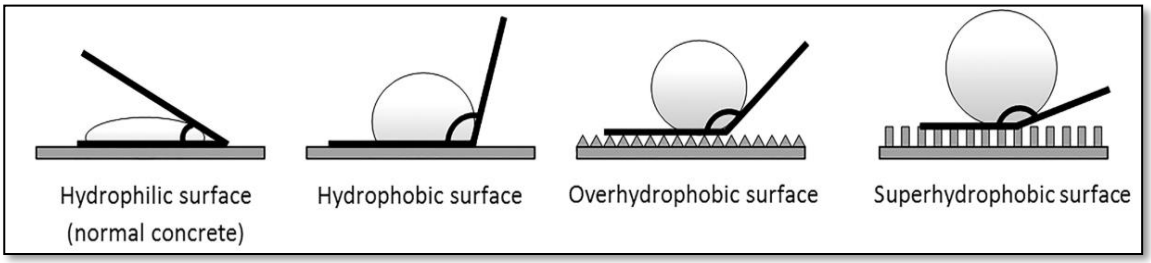

Figure 2: Contact angle and surface - Reprinted from (I. Flores-Vivian, 2013)

Compared to other hydrophobic agents, silane has smaller molecules which permits them to enter small pores, issuing in more effective surface treatments. These agents, in addition to their hydrophobic effects on the surface of the concrete, reduce the effect of freeze/thaw and minimize the bond between the concrete and the freezing water (Gao, Deng, & Yang, 2011). The silane structure is given in Figure 3a. Figure 3b shows the global structure of silane derivatives, where R can either be an alkyl, aryl or even any other organo-functonial group. OR' generally designates an alkoxy functional group or a hydroxyl group (OH) or salt (ONa).

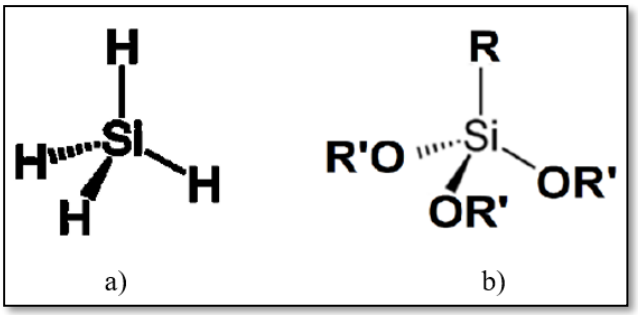

Figure 3: Silane structure (a), General structure of silane derivatives (b)

Based on sodium silicate, the inorganic surface treatments act as pore-blocking components. In contrast to the organic surface treatments, the inorganic treatments are more stable and resist aging but do not generate a hydrophobic layer. They are usually used to improve the abrasion resistance of the concrete pavement surface exposed to repetitive traffic loading. Typical inorganic surface treatment agents embrace potassium silicates, sodium silicate solution and fluosilicates (Bertolini, Elsener, Pedeferri, Redaelli, & Polder, 2013). The lithium silicate for e.g. reacts chemically with hydrated lime (calcium hydroxide), which is available at the surface of the concrete to create Calcium-Silicate-Hydrate (CSH) gel, an insoluble wear and moisture protective surface. Normally, this lime is produced during the hydration of the cement and, in improper curing conditions, is suspended in the pore water and deposited on the surface as the water evaporates (ACI.2R-01, 2001). As a result of this reaction, the hardness and impermeability of the concrete surface layer increase (Thompson, Silsbee, Gill, & Scheetz, 1997).

4. Assessment of the efficiency of concrete surface treatments

a) Petrographic analysis

In this dissertation, a qualitative analysis that embraces the assessment of interconnected capillary voids, carbonation and cracks will be done to identify the impact of a surface treatment on the microstructure of a concrete.

A petrographic analysis is a study to examine samples of rocks or concrete and consequently be able to determine their mineralogical and chemical compositions. The

observations are accomplished using a polarizing microscope that requires the use of polarized light to scrutinize the optical properties of various specimens. Originally it has been used in the domain of geology. When Le Chatelier reported the presence of abundant clear colorless tricalcium silicate, dicalcium silicate, calcium alumino-ferrite and tricalcium aluminate using the polarizing microscope, this technique introduced a new era in the study of Portland Cement Concrete constituents. The petrographic study of concrete has a wide history, as depicted by the review published by Mielenz (Mielenz, 1962). The ASTM C 856 (ASTM C 856, 2018) outlines the steps for petrographic of samples of hardened concrete and how they can be examined and extracted from existent concrete structures. In addition, the ASTM C 457 (ASTM C 457, 2016), reports the procedures for microscopical determinations of specific surface, void frequency, spacing factor, air content and paste-air ratio of the air-void system. An optical microscopic analysis permits the investigation on the structure of cement paste, aggregates, micro voids and cracks in addition to the carbonation of aggregates (Georgali & Tsakiridis, 2005). In his review, W.J. French showed a detailed report of observations made on actual samples in order to evaluate quantitative information (French, 1991).

b) X-Ray fluorescence

The X-Ray fluorescence (XRF) is a non-destructive elemental analysis technique for quantification of nearly any element applied on the surface. This analytical method permits to identify and quantify the chemical composition of the materials, which can be solid, liquid or powder. Through its high precision, an XRF gun is capable of determining the thickness of multiple layers and coatings. Usually, the measurement time depends on

the number of elements and the required accuracy. Using a handheld XRF gun, this time varies between seconds and 30 minutes. The tool is cost-effective since the cost of well-conducted testing and quality control is smaller compared to the cost of removing and replacing failed concrete structures. In the concrete industry, the XRF has been widely used and especially for quality control (QC) related to cement production. This test gives an accurate analysis in evaluating the raw materials, estimating the intermediate products such as the clinker and gypsum, and checking the required standards for cement production according to ASTM.

Moreover, the XRF technique is able to assess the proportions of concrete mixtures and cementitious materials (Taylor, Yurdakul, & Ceylan, 2012) . Researchers used this device to study the properties of new concrete structures with recycled concrete aggregate (RCA) to compare the chemical composition between the RCA and natural aggregates (M.C.Limbachiya, E.Marrocchino, & A.Koulouris, 2007). Durability concerns have been treated by evaluating the initiation time to corrosion in reinforced concrete structures due to chloride penetration and estimating the remaining time. This has been done by characterizing the depth of penetration of the chloride ions using the XRF (Proverbio & Carassiti, 1997). In the study reported herein, the XRF gun is used to determine the different elements at the surface of a concrete specimen treated with a chemical and their depth of penetration. In order to determine the concentration of intended elements, the test is required to be implemented at depth intervals since only the atoms within the analysis depth are analyzed.

c) Water sorptivity index

The deterioration of concrete pavements is usually affected by the transport of detrimental elements such as sulfate ions, chloride and water into the concrete. Although, permeability is an indicator of a concrete pavement's capacity to carry water, oxygen or carbon dioxide, two mechanisms actually control the absorption and transport of water. *Permeability*, an indicator of the flow of water under pressure in a saturated porous material, and *Sorptivity*, which characterizes the material's potential to absorb and transmit water through it by capillary suction (Sabir, Wild, & O'Farrell, 1998). The sorptivity can be defined then as the rate of movement of water through a porous material under capillary action. This phenomenon has been studied by many researchers in order to come up with models and computational tools to predict the service life of concrete pavements (Bentz, Ehlen, Ferraris, & Garboczi, 2001). There are different methods to evaluate the absorption of mortar specimens and although these methods are very efficient, little in the literature has shown their application to evaluate a surface treatment's ability to repel water or decrease the absorption capacity of a concrete surface. After conditioning, only the top surface of the specimen will be in contact with water and all the other sides sealed. Consequently, the absorption rate is a function of the change in specimen mass, the exposed area of the specimen and the density of water according to the following equation:

$$I = \frac{m_t}{a * d}$$

Where:

I = The absorption,

m_t = The change in specimen mass in grams, at the time t,

a = The exposed area of the specimen in mm^2,

d = The density of the water in g/mm^2.

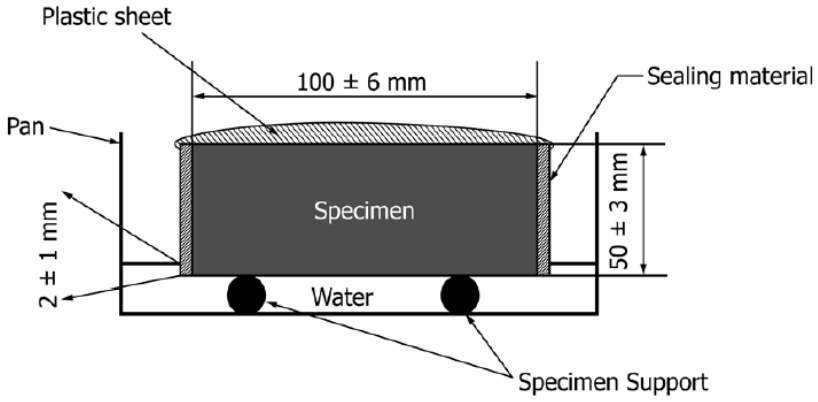

Figure 4: Schematic of the procedure (ASTM C 1585, 2011)

d) Rapid chloride penetration

Chloride penetration is one of the main factors affecting the durability of reinforced concrete structures due to corrosion of the steel reinforcement. For corrosion to take place, four conditions must be met: High chloride concentration at the level of the rebar, presence of moisture, presence of oxygen and high electrical conductivity. Due to the high pH of the hydration products, the steel is usually protected from corrosion and the level of

corrosion is therefore negligible. The penetration of chloride ions appears either through the capillary pores or through the cracks by capillary suction, diffusion or simply by permeation (Hilsdorf & Kropp, 1995). The diffusion of the chloride ions in the concrete decreases the pH to a level at which the oxidation reaction for corrosion can occur ($pH < 9$). The oxidation that takes place within the concrete structure has dual adverse effects. The first effect is the reduction of steel cross section that may cause to uneven areas of steel required for carrying applied load. In addition, the rust occurred due to this oxidation will have notably higher volume than the original steel which leads to an increase of the internal stresses on the surrounding concrete causing it to crack and spall. One of the methods to identify the chloride penetration depth is by spraying 0.1 N silver nitrate aqueous solution on a cross section of split concrete (Otsuki, Nagataki, & Nakashita, 1992). It has been shown that a good quality of concrete has a lower chloride penetration and the penetration depth increases with the length of exposure (Meck & Sirivivatnanon, 2003). Moreover, Costa *et al* showed that the surface chloride content is not influenced by the concrete quality but it is greatly affected by the exposure conditions (Costa & Appleton, 1999).

Other than the use of a solution of silver nitrate to identify the chloride presence, the ASTM C 1202 (ASTM C 1202, 2017), depicts a method that covers the determination of the electrical conductance of concrete to provide an indication of its resistance to chloride ions penetration. This test has proven to be an efficient test method for different types of concrete. Elsalamawy studied the efficiency of different surface treatments and crystallization materials in reducing chloride ions ingress in concrete (Elsalamawy,

Mohamed, & Abosen, 2017). It has been shown that the most effectiveness of the crystallization coating materials was only determined with old concrete specimens (3-4 months).

In the study reported herein, the surface treatments used are organic and inorganic treatments. A correlation of their different effectiveness will be established according to the rapid chloride penetration test.

CHAPTER III

LABORATORY TESTING

1. Overview

The following test program aims to present an overview of the durability of the surface of concrete and mortar specimens regarding abrasion and freeze/thaw cycles. It introduces different laboratory testing to assess the efficiency of organic and inorganic surface treatments. A total of 6 mixture designs were assigned; two of them are concrete mixture proportions and 4 mortars. The different types of surface treatments used throughout the test program are explained in the following section.

2. Surface treatments and applications

A combination of surface treatments was provided by the manufacturer and are detailed in the following table (Table 1).

Table 1: Surface treatments and type

Name	Type
TRANSIL 5561/PLUS	Inorganic
TRANSIL 5560	Inorganic
TRANSIL 6400	Unknown
SILANE Z-6341	Organic
SILANE 6595	Organic

The TRANSIL 5561/PLUS is a surface treatment clear, penetrating, breathable, surface-applied liquid treatment which strengthens, protects and hardens concrete pavements in cold climates subjected to freeze-thaw cycling, studded tires, and deicers. It is a concrete wear resistant surface hardener with anti-scale protection that is a low viscosity surface treatment that penetrates the wear layer of concrete. It is an inorganic surface treatment that combines lithium silicate chemistry with reactive silicon catalysts. Mostly water-based, this chemical combination forms an extremely hard and abrasion resistant compound which provides both increased abrasion resistance and moisture protection, making concrete more durable and less prone to scaling, spalling and deterioration from traffic wear.

The TRANSIL 5560 protects and hardens concrete pavements. Its high performance to maximize durability and longevity of tined, diamond ground, grooved, milled and shot-blasted makes the surface less prone to rutting and early wear. TRANSIL 5560 penetrates the wear layer of concrete, where it reacts with the free lime to form calcium silicate hydrate and consequently leads to an insoluble wear and moisture protective surface. Apparently, the only difference between this surface treatment and the TRANSIL 5561/PLUS is that it has low effect on protecting the concrete pavement against freeze/thaw cycles.

Concerning the TRANSIL 6400, its chemical composition is based on silicon and will be used as a post product applied on the top of a surface treatment. The Silane Z-6341 and Silane 6595 are both organic treatments and perform well in reducing water penetration by making the surface hydrophobic.

3. Concrete and mortar constituents, mix designs, and curing

a) Concrete mixture proportion

Two concrete mix designs were utilized for this study. An ASTM specification C 150-07 (ASTM C 150-07, 2007) Type I/II Portland cement was used. Two types of coarse aggregates were present with a maximum size of 25mm. The fine aggregates consisted of natural, clean silica sand with a maximum size of 4.75mm. Class C fly ash was added as a 40% cement replacement (ASTM C 618, 2008). The aggregates' specifications were determined according to the ASTM C 127 (ASTM C 127, 2004) and ASTM C 128 (ASTM C 128, 2004). The mix proportion of concrete is summarized in Table 2.

Table 2: Concrete Mixture Proportions vs. TRANSIL 5561/PLUS

Mixture Component	Quantities lbs./yd^3	
	Mix design 1	**Mix design 2**
Cement	395	395
Fly Ash	169	169
River Gravel	1765	0
Limestone	0	1763
Sand	1243	1167
Net Water	224	231
	w/c = 0.44	
	Coarse Aggregate Factor = 0.68	
	No air entraining and admixtures	

The coarse aggregates were washed to remove all dirt and then were added to the sand in the mixing container. The cement and fly ash were added to the mixture. When a

homogenous mix was obtained, the water was finally added. The batch was remixed periodically until the concrete was homogenous and reached the desired consistency according to the ASTM C 192 (ASTM C 192, 2007). As recommended for any freeze/thaw test, the designed air content for the two mix designs was fixed at 6.0%. For each mix, the concrete specimens were cast in plastic squares (6 × 6 in.) and in cylinder molds (4 × 8 in.).

b) Mortar mixture proportion

Concerning the mortar mixture procedure, the ASTM C 305 (ASTM C 305, 2014) was adopted and the four mix designs are showed in the following tables (Table 3-4).

Table 3: Mortar mixture proportions 3&4

Mixture Component	Quantities lbs./yd^3	
	Mix design 3	**Mix design 4**
Cement	923	974
Fly ash	277	292
Sand	2521	2661
Net Water	315	239
w/c	0.48	0.38

Table 4: Mortar mixture proportions 5&6

Mixture Component	Quantities lbs./yd^3	
	Mix design 5	**Mix design 6**
Cement	1080	1123
Sand	2145	2230
Net Water	535	438
w/c	0.48	0.42

4. Test program

The test program exposed in the following section consists of testing different combinations of surface treatments regarding their efficiency to improve the resistance to abrasion and freeze/thaw cycles of the concrete mixtures (Mix 1&2) and mortar specimens (Mix 3&4). Mix 5 & 6 will be used to assess the effect of the surface treatments on the porosity of surface.

a) Specimen preparation

Table 5 summarizes the specimens used in this study for Mix 1&2. All specimens cured in a controlled room at 20˚C and 100% Relative Humidity for 28 days. The specimens with river gravel reached a compressive strength of 4,900 psi. The specimens with limestone had a compressive strength of 5,900 psi at 28 days. Mix 3 (w/c = 0.48) had a compressive strength of 3,789 psi and Mix 4 (w/c = 0.38) a compressive strength of 4,816 psi. A dike about 25 mm wide and 20 mm high was placed along the perimeter of

the surface of the specimens subjected to the freeze/thaw test in order to prevent any possible deicer solution leaks. This dike was adhered to the edge of the specimens by using a waterproof epoxy.

Table 5: Specimens Mix 1&2

Specimens	Shape	Dimensions (in^2)	ID	Number of specimens	Type of test
Control	Square	6 × 6	$C_{N/F}$	1	Abrasion
	Square	6 × 6	$C_{F(15)}$	1	15 cycles Freeze/thaw
Treated	Square	6 × 6	$T_{N/F}$	2	Abrasion
	Square	6 × 6	$T_{F(15)}$	2	15 cycles Freeze/thaw

Figure 5: Specimens cylinder

Figure 6: Specimens shape and preparation

b) Surface treatments applications

After 28 days, the specimens were exposed at 23 +/- 2˚C and 50% relative humidity for 24h. The surface treatment was applied at a rate of 175 ft^2/gallon to the top surface of the specimens, followed by a 24h drying period. The control specimen has not been treated. The following table exposes the different types of surface treatments used.

Table 6: Specimens and surface treatments

Mixture	Surface Treatment	ID	Test performed
1 & 2	TRANSIL 5561/PLUS	Refer to Table 5	Refer to Table 5
3 (w/c = 0.38)	TRANSIL 5560 + TRANSIL 6400	T5560/6400	Abrasion
	TRANSIL 5561 + TRANSIL 6400	T5561/6400	
	TRANSIL 5561/PLUS	T5561	
	Silane Z-6341	S6341	
	Silane 6595	S6595	
4 (w/c = 0.48)	TRANSIL 5560 + TRANSIL 6400	T5560/6400	Freeze/Thaw
	TRANSIL 5561 + TRANSIL 6400	T5561/6400	
	TRANSIL 5561/PLUS	T5561	
	Silane Z-6341	S6341	
	Silane 6595	S6595	
5 & 6	100 % Silane Z -6341	100%Z6341	Refer to table 7
	40 % Silane Z-6341	40%Z6341	
	TRANSIL 5561/PLUS	T5561	
	TRANSIL 5561 + TRANSIL 6400	T5561/6400	
1 - 6	None	Control (C)	All tests

Table 7: Test program Mix 5&6

Test	Specimen Shape	Dimensions (in)	Standard
Water sorptivity index test	Cylinder	4×2	ASTM C1585
Rapid chloride migration test (RCMT)	Cylinder	4×2	ASTM C1202
Microscopical analysis	Slide	2×3	ASTM C856
X-ray fluorescent (XRF)	Cylinder	4×4	ASTM D5381

c) Abrasion test

The abrasion test was based on the ASTM C 944 (ASTM C 944, 2006) as a means to simulate the effects of wear on roads under the action of chains and metal wheels. This test consists of a drill press with a chuck capable of holding and rotating the abrading cutter at a speed of 200 rpm and exerting a force of a normal load of 44 ± 0.4lbf. In this study, a constant load is used during 3 cycles of 2, 4 and 6 minutes. At the end of every cycle, a high-pressure air blower was used for cleaning up the loose dust to prepare the specimen to be weighed. The cumulative mass loss was consequently determined.

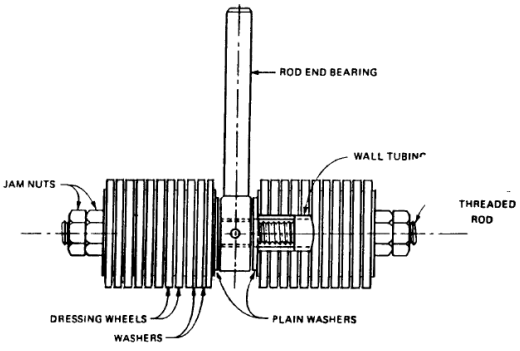

Figure 8: Typical rotating cutter (ASTM C 944)

Figure 7: Abrasion machine

d) Salt scaling test

An abbreviated method of the ASTM C 672 (ASTM C 672, 2012) was used to perform this test. After 28 days, 6 mm of a solution of a 4 wt. % deicer calcium chloride was added at the surface of the specimens. The specimens were alternately placed in a freezing environment at -18˚C for 16h then allowed to thaw at 23˚C for +/- 8h which corresponds to a single cycle. Unlike the ASTM C 672 that uses a visual rating system, a modified approach recommended by the Strategic Highway Research Program (SHRP) and Canadian Standards Association (CSA) was performed. Water was added between each cycle to maintain the proper depth of solution. After every five cycles, a visual assessment was made and the specimens were flushed with tap water. The eroded aggregates and paste were washed into a funnel with a filter paper inserted. The filter paper was dried at 38˚C overnight and the weight was recorded. The cumulative weight loss from the exposed aggregate surface is considered to be an indication of the severity of the deicer chemical and the efficiency of the surface treatment used. The test was conducted for 15 cycles.

Figure 10: Environmental machine

Figure 9: Specimens in the environmental chamber

The objective of the following tests done on the specimens from Mix 5&6 is to examine microscopically different combination of surface treatments (Table 6) with respect to:

1. The chemical elements at the surface using an X-ray fluorescence analyzer (XRF)
2. Their capacity to repel water or reduce the size of the pores by performing the water sorptivity test.
3. Their efficiency regarding the chloride ions penetration in the concrete sample through the surface.
4. A qualitative analysis of the interconnected capillary voids, the bleeding channels and carbonation. In addition to a study of the area and density of the voids by performing a petrographic analysis on thin section of the concrete samples.

A subjective correlation between the results of each assessment should enhance the understanding of the function of these surface treatments and their capacity to improve abrasion and freeze/thaw damage.

e) Water sorptivity test

After curing, the 4×8 (in) cylinders were reduced to 4×2 (in). The objective of this test is to determine the susceptibility of an unsaturated concrete to the water penetration following the ASTM C 1585 (ASTM C 1585, 2011) procedure. This method differs from the test depicted in the ASTM C 642 (ASTM C 642, 2013) where the specimens are completely immersed in the water after being oven dried. In this test method, only the surface is exposed to water at room temperature while the other surfaces unexposed are sealed. The absorption is consequently unidirectional. The test started by conditioning the samples. After curing, every sample is put separately in a desiccator connected to a pump

in order to remove all the air from the voids for a duration of 30mins (Figure 11). Consequently, the surface of the specimen will have a higher pressure than the pores' and this will allow a direct suction of the water at the surface of the concrete specimen. Following that, all the sides of each specimen were sealed with duct tape and the mass of the conditioned specimen recorded in addition to the area of the specimen in contact with the surface of the water.

Figure 11: Desiccator for conditioning

Figure 12: Samples in the pan

A support device was built at the bottom of the pan after it has been filled with water (1 to 3mm above the top of the support device). The specimens were put upside down on the support device and whenever in contact with the water (no more than 2mm), the timing device started. Every time intervals, the specimen were removed from the pan, the timing device stopped and a dry towel was used to tap the surface and remove the excess of water. Following that, the specimen's mass was determined using an electronic scale. After the mass was recorded, the specimens were immediately put again in the pan. The test lasted

for 10 days. The following figures (Figure 13-15) show the contact angle of a drop of water at the surface of the treated and untreated specimens.

Figure 13: Drop of water at the surface of two specimens at t = 0mins

Figure 15: Same drop of water after t = 5mins

Figure 14: Upper view of the two specimens after t = 10mins

f) X-Ray fluorescence analyzer test

The XRF is a non-destructive elemental analysis technique for quantification of nearly any element applied on the surface. This analytical method permits to identify and quantify the chemical composition of the materials, which can be solid, liquid or powder. The purpose of the test performed in this section is to assess the chemical composition at the top of the treated surface and try to quantify the permeation of the surface treatment by identifying the elements at a certain depth. The specimens tested were reduced to a height of 2-3in after they have been treated with the designated product. The test was based on the ASTM D 5381 (ASTM D 5381) and following the instructions provided by the manufacturer of this instrument.

Before the test, the instrument was calibrated using a stainless steel #316 discs to check the operation of the XRF instrument. The test started first by isolating the solid supported by briquettes on a table. The first attempt was the application of the XRF directly at the surface of the specimen followed by several attempts made at different depth intervals (every 2mm) (Figure 16). Once the test was performed, the data was visible on the screen of the analyzer with the different chemical elements and their associate percentages. The analyzer was connected to a computer in order to collect all the data after the test.

Figure 16: XRF Test

g) Petrographic analysis test

A petrographic analysis is a study accomplished using a microscope to examine samples of rocks or concrete and consequently be able to determine their mineralogical and chemical compositions (Figure 17). The microscopical analysis is a very useful technique to provide useful data on the analysis of the cement, concrete and other construction materials. Microscopy is a convenient method in order to understand the mechanism of the concrete structure by combining complementary techniques like electron microscopy and chemical analysis.

The test was performed on 10 sections (5 samples from each mix design). The concrete specimens were sent to National Petrographic Service, Inc. in Rosenberg in order to make the thin sections. The procedure for the petrographic examination of the samples of hardened concrete was done according to ASTM C 856 (ASTM C 856, 2018). Many features can be made regarding the materials coherence, the air voids, the nature of the external surface, the coarse aggregate type, the nature of the different types, the size range and distribution of the voids etc. For this study, we were interested in making a qualitative analysis of the interconnected capillary voids, the bleeding channels and the carbonation rate. Consequently, we would be able to understand the effect on a microscopic scale of the different combination of surface treatments applied on the surface of the cured concrete samples. In addition, the results obtained during this test will be correlated to the other results of previous test in this phase of this study.

Figure 17: Petrographic microscope

h) Rapid chloride penetration test

The objective of this test is to determine the electrical conductance of concrete samples in order to provide a rapid indication of its resistance to the penetration of chloride ions. This penetration occurs through the capillary pores, the cracks by permeation, the diffusion and also the capillary suction. The experiment consists of controlling the amount of electrical current passed through 50mm thick slices of 100mm nominal diameter cylinder according to ASTM C 1202 (ASTM C1202, 2017).

The main materials used are the following: Specimen-Cell Sealant, Sodium Chloride Solution – 3.0%, Sodium Hydroxide Solution – 0.3 N, an applied voltage Cell, a data Readout Apparatus.

Conditioning

Since ingress of chloride ions into concrete only takes place when the pores of the specimen are fully or partially filled with water, conditioning is an important phase of the experience. All specimens (treated or not) cured for 56 days before testing. The specimens were put in a vacuum desiccator with both end faces exposed. Using a pump, the pressure inside the desiccator decreased to less than 50mm Hg for 3 hours (Figure 18). While the vacuum pump was still running, water was added to the container. Once the pump was turned off, the specimens were let soaked in the water for 18 hours.

Procedure

The specimens were removed from the container, mounted on the two cells and sealed with epoxy. One side was filled with 3.0% NaCl and the other with 0.3 N NaOH. Electrical connections were made to voltage application and data readout apparatus. Once everything was set, the power supply was turned on and set to 60 V. Every 30mins, a reading of the data was made for a total of 6 hours (Figure 19-20).

Figure 18: Pump connected to a desiccator

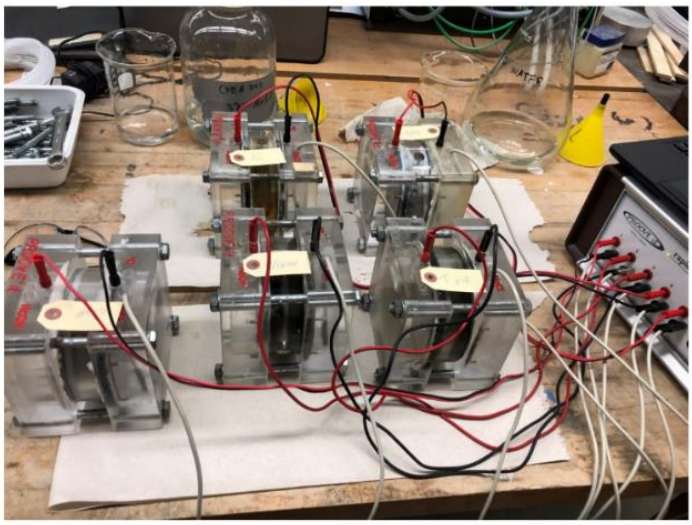

Figure 19: Specimens sealed to the cells

Figure 20: Readings obtained during the test

CHAPTER IV

RESULTS, ANALYSIS AND DISCUSSION[2]

1. Test results

a) Abrasion of concrete

The abrasion resistance of surface-treated concrete is an indicator of the longevity of the surface treatment under repetitive traffic loading. However, when the surface is completely worn away, the abrasion resistance depends on many other factors such as the abrasion resistance of the aggregates, their shape and sizes. During the entire test, the surface treatment used showed a significant impact on improving the abrasion resistance of the concrete surface (Figure 21). For the mix with river gravel, the surface treatment performed well during the whole test and especially during the first 4 minutes where only the surface was abraded. By contrast, the control limestone mixture showed more damage during the first 2 minutes. Following that, the results were mixed. The limestone demonstrated an anisotropic behavior during the test, which illustrates a lack of homogeneity underneath the abraded layer. It was predicted that the samples with limestone would exhibit less loss damage since they had a higher compressive strength than the samples with river gravel. As the compressive strength increases, the resistance to abrasion increases and consequently leads to a lower mass loss. Moreover, the coarse

[2] Part of the contents in this chapter is reprinted with permission from:
An approach to characterize the wearability of concrete pavement surface treatments, by Abou Sleiman C., Shi X., and Zollinger D., Transportation Research Record: Journal of the Transportation Research Board, 2019. DOI: https://doi.org/10.1177/0361198118821668.

aggregate factor had a major role regardless of the type of aggregates used. The wear resistance of concrete pavement depends on the proportion of coarse aggregates adopted; a concrete specimen with a high coarse aggregate factor will exhibit less loss damage due to abrasion. In addition, the downward pressure applied during the test had a significant impact in the mass loss results. The chemistry of this specific surface treatment based on reactive lithium and silicon enhanced the bonding with calcium hydroxide to lead to a better quality and tougher concrete surface.

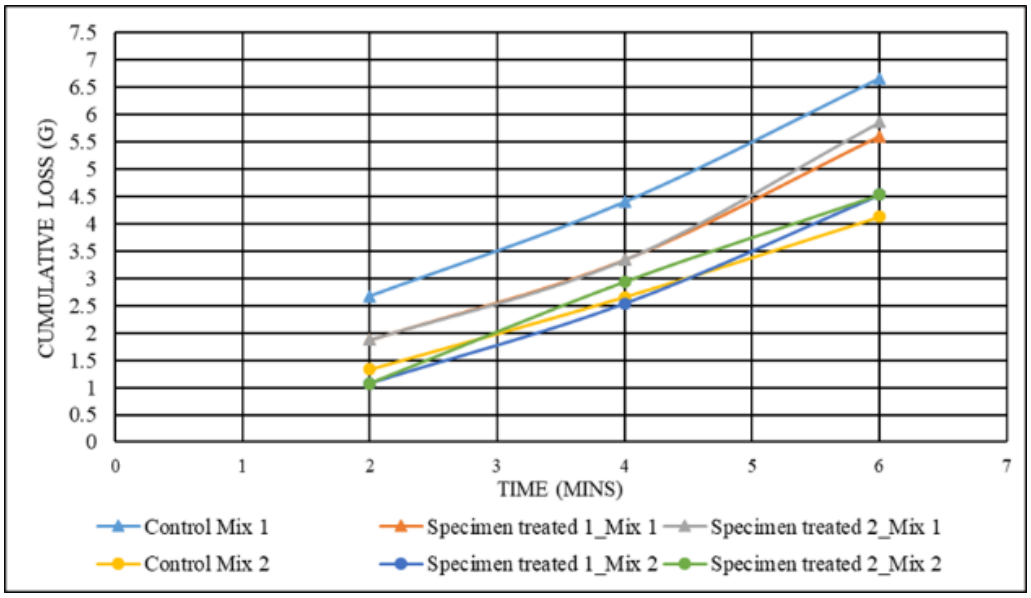

Figure 21: Cumulative mass loss for Mix 1&2

b) Abrasion of mortar

In order to prevent the effect of the choice of aggregates on the abrasion resistance, the abrasion test was performed on mortar specimens. The abrasion resistance of a concrete pavement surface is related to the quality of the surface whenever it is eroded, permeable or soft. As described by the manufacture, the two types of TRANSIL

(TRANSIL 5561/PLUS and TRANSIL 5560) which are inorganic surface treatments maximize the longevity of a concrete pavement surface under abrasion due to tires. Results from the abrasion test are presented in the following figure (Figure 22). The TRANSIL, regardless its type, showed less cumulative mass loss than the control and Silane specimens. In addition, the post treatment TRANSIL 6400 increased the resistance to abrasion if a comparison between the T5561/T6400 and T5561 is made.

By comparing the T5560/T6400 and T5561/T6400, it is clear that the T5560 doesn't have the same effect as the T5561 regarding its capacity to protect from abrasion. Moreover, the specimens treated with Silane (S6341 and S6595) – organic surface treatment showed an equivalent cumulative mass loss compared to the control specimen.

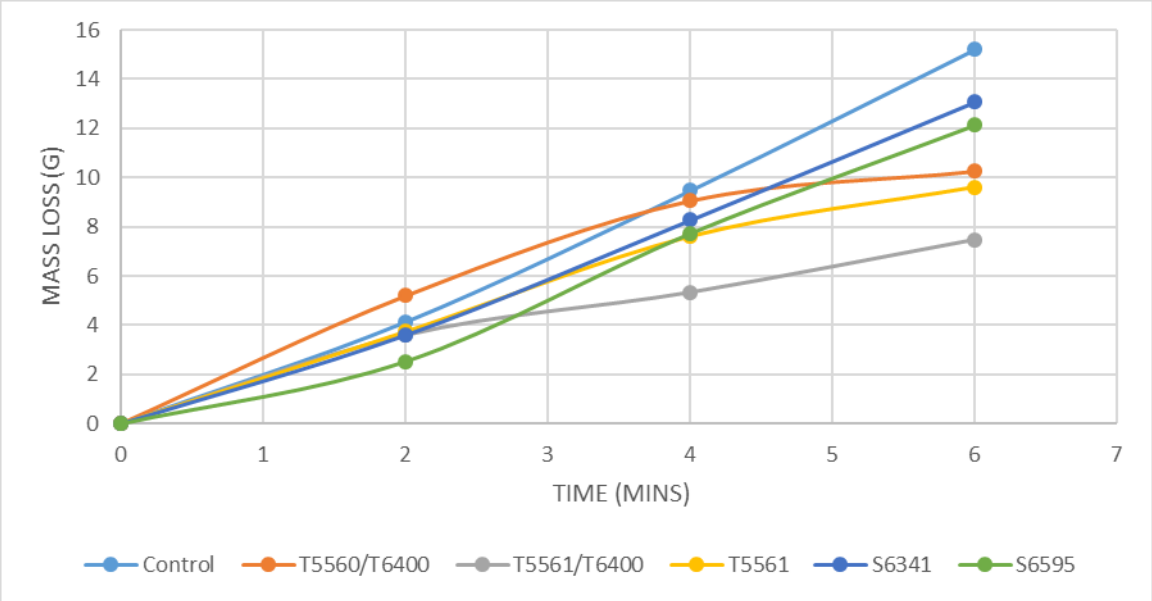

Figure 22: Cumulative mass loss due to abrasion Mix 3

c) Scaling resistance of concrete exposed to freeze/thaw and deicer chemical

Every 5 cycles, the surface of the specimens was washed and the cumulative weight loss was measured. This mass loss is an indicator of the longevity of the surface treatment. During the 15 cycles and for the two mix designs, the untreated specimens showed a significant mass loss compared to the treated concrete specimens (Figure 23). The mass loss was more significant during the 15 cycles for the specimens with river gravel than for the ones with limestone (Figure 23 - 25). This additional result asserts that the aggregate characteristics control the frost damage. The gravel aggregates were larger than the limestone aggregates. Under freezing conditions, the unfrozen water in smaller aggregate particles is expelled quickly without developing damaging pressure within the structure of the concrete. Pore structure (i.e., pore size, pore shape and pore distribution) is also an indicator of the performance of an aggregate under freeze/thaw cycles.

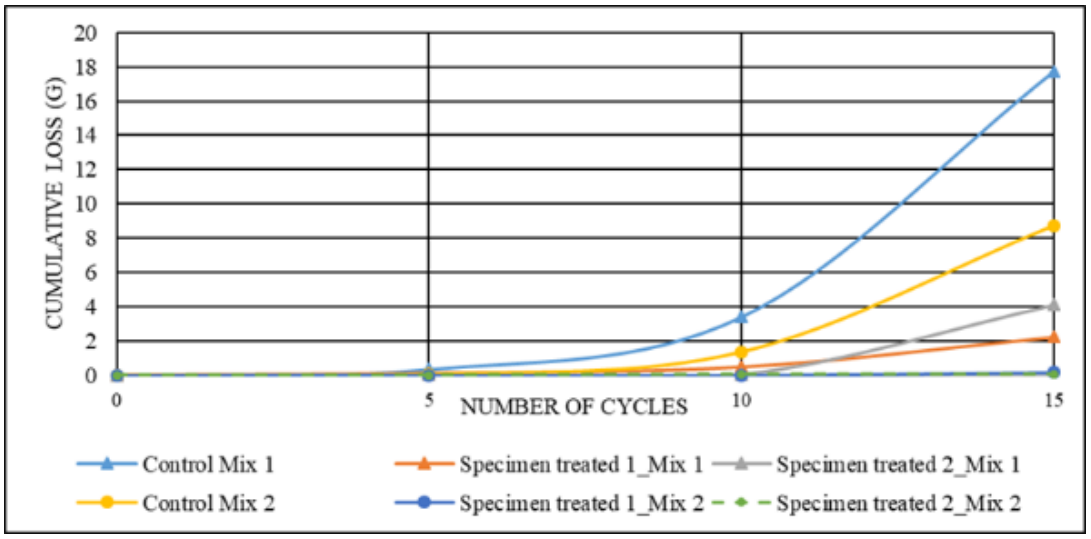

Figure 23: Cumulative mass loss for Mix 1&2

Figure 24: Results for the mix with river gravel after 15 cycles

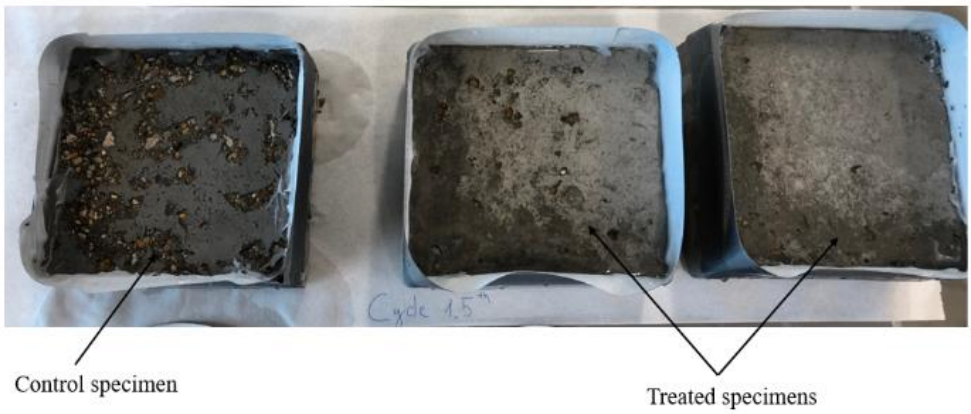

Figure 25: Results for the mix with limestone after 15 cycles

d) Scaling resistance of mortar exposed to freeze/thaw and deicer chemical

The freeze/thaw test was conducted on concrete specimens with a w/c = 0.48 for a period of 20 cycles. According to the results (Figure 26), the two types of Silane (S6595, S6341) and the T5560/T6400 showed no cumulative mass loss during the whole test. The TRANSIL 5561/PLUS (T5561) showed more mass loss than the TRANSIL 5561/PLUS with the post surface treatment TRANSIL 6400 (T5561/T6400) (Figure 27-29). The post

treatment increased the resistance to freeze/thaw. The untreated specimen had a higher cumulative mass loss than all the other specimen.

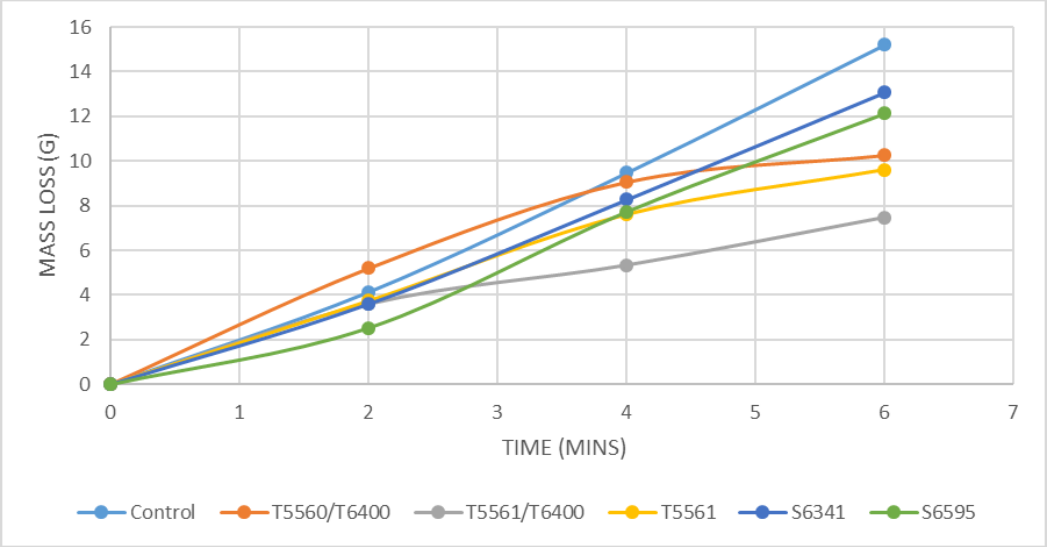

Figure 26: Cumulative mass loss due to freeze/thaw for Mix 4

Figure 27: Control specimen and TRANSIL 5561/PLUS

Figure 28: T5560/T6400 and T5561/T6400

Figure 29: S6595 and S6341

e) Freeze/thaw test on abraded mortar specimens from Mix 3

The following test was performed on the specimens subjected earlier to the abrasion test. These specimens have a w/c = 0.38. This procedure simulates the action of the metal wheels on the concrete pavement and its exposure to freezing and thawing conditions. The test was conducted for 20 cycles. The results appear in the following figures (Figure 30-31).

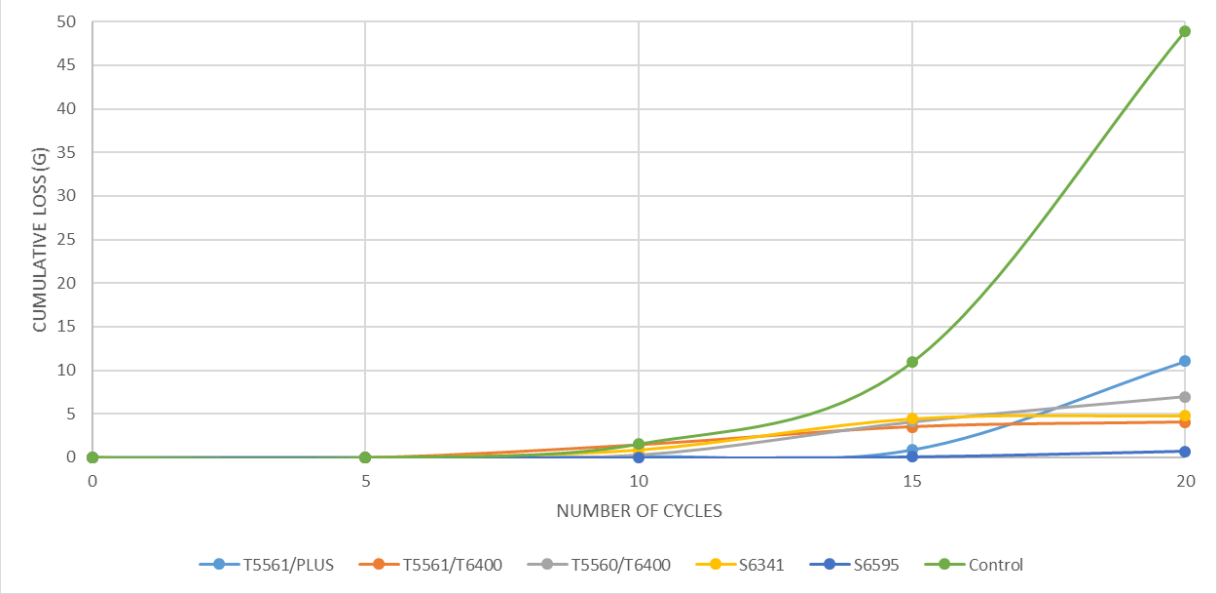

Figure 30: Cumulative mass loss due to freeze/thaw on abraded specimens

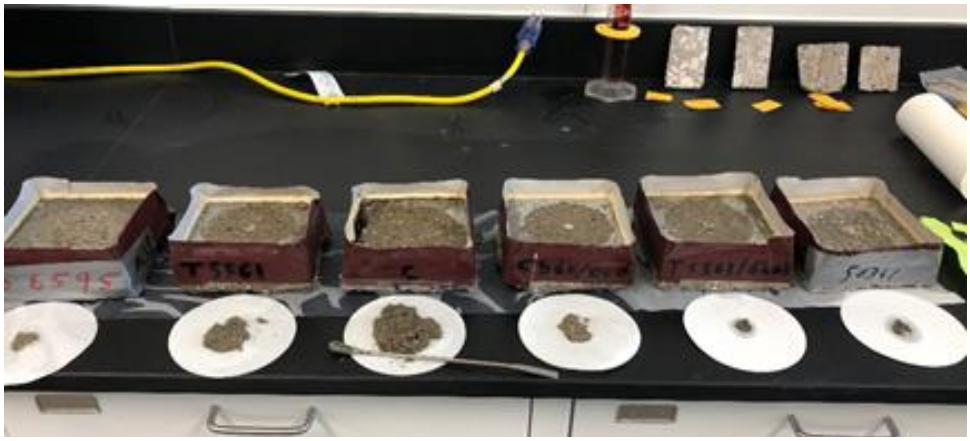

Figure 31: Visual assessment of Freeze/thaw damage and mass loss collection

The control specimen showed more mass loss due to freeze/thaw cycles than all the other specimens. According to the results obtained, the surface treatments were not totally worn away due to the abrasion test since the resistance to freeze/thaw of the specimens can still be remarkable. During the abrasion test, the specimens treated with the Silane showed an equivalent mass loss compared to the untreated specimen. During the salt scaling test, the difference between these two mass losses increased significantly. This is an indicator that the silane could have entered the pores of the concrete where its efficiency was noticeable.

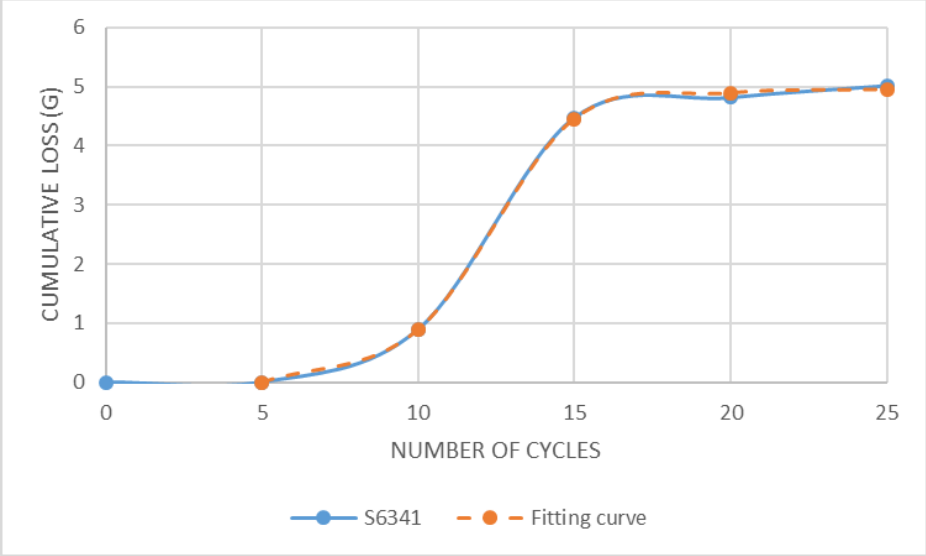

Figure 32: Fitting curve of the cumulative mass loss

f) Water sorptivity test

At a given time-intervals, the change in mass of each specimen was recorded in order to calculate the absorption, *I*, given by the following equation.

Where:

$$I = \frac{m_t}{a * d} \quad (1)$$

Where:

I = The absorption,

m_t = The change in specimen mass in grams, at the time t,

a = The exposed area of the specimen in mm^2,

d = The density of the water in g/mm^2.

The initial absorption rate of water ($mm/s^{1/2}$) can be determined as the slope of the line that is the best fit to *I* plotted as a function of the square root of time ($s^{1/2}$) using a regression analysis from 1min to 6h. If the data doesn't show a linear relationship, the initial rate cannot be determined.

The secondary absorption rate of water ($mm/s^{1/2}$) can be determined as the slope of the line that is the best fit to *I* for the data between 1 to 7 days.

Both absorption rate can be used to evaluate the connectivity of the pore network. The following figure (Figure 33) shows the result for the control specimen of the mix design with w/c = 0.48. All other graphs are in the Appendix A.

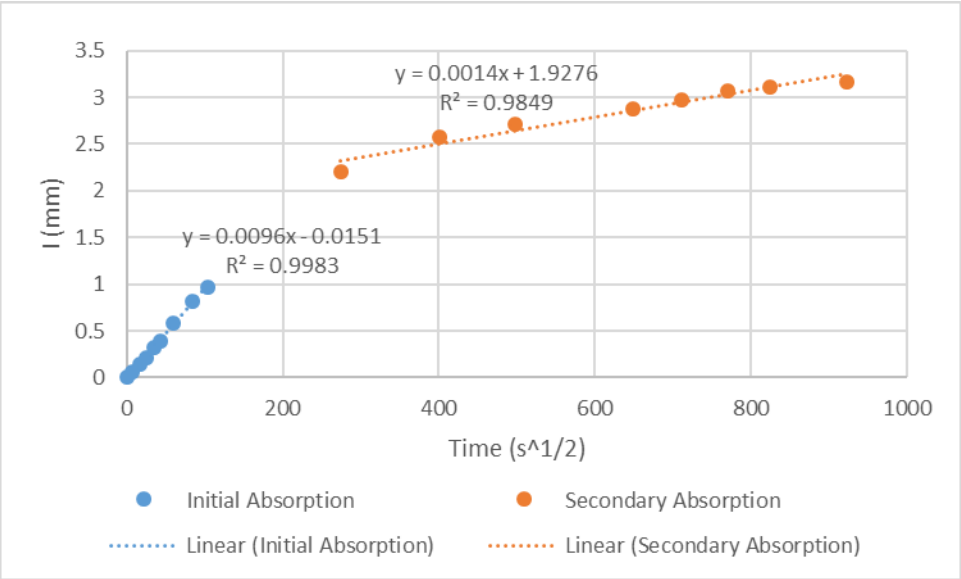

Figure 33: Absorption of the Control sample (w/c=0.48)

The following figures (Figures 34-37) summarize both initial and secondary rate of absorption for each sample and for each mix design.

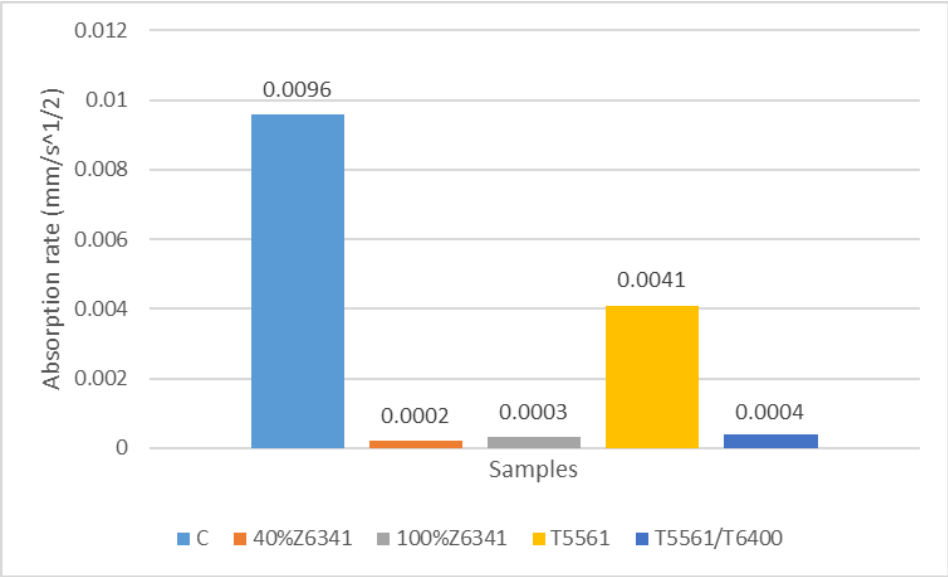

Figure 34: Initial rate of absorption - Mix design 0.48

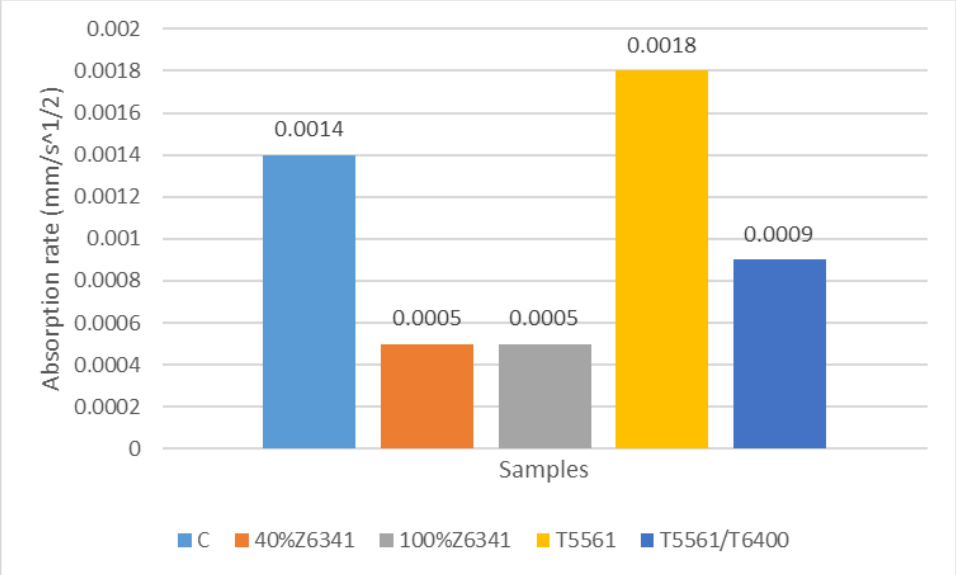

Figure 35: Secondary rate of absorption - Mix design 0.48

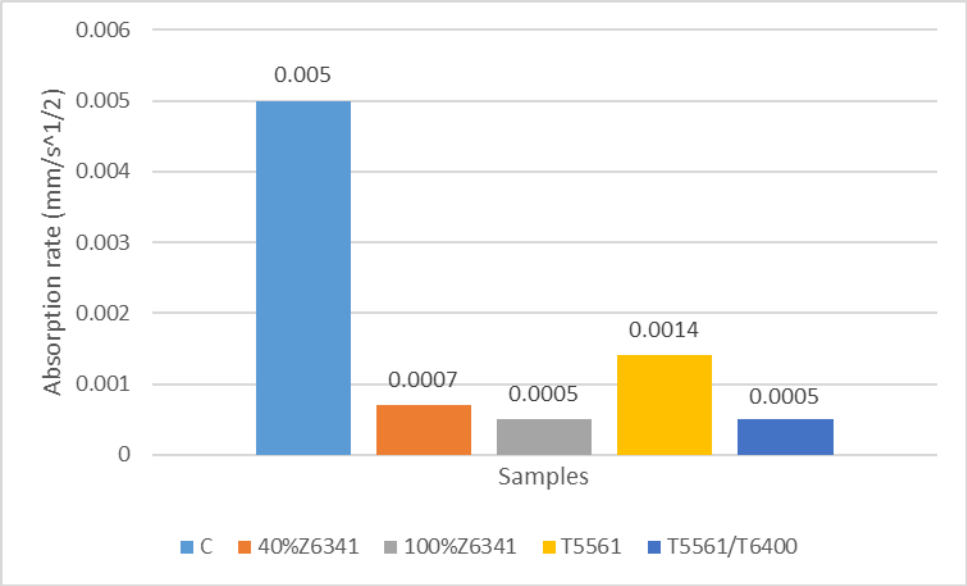

Figure 36: Initial rate of absorption - Mix design 0.42

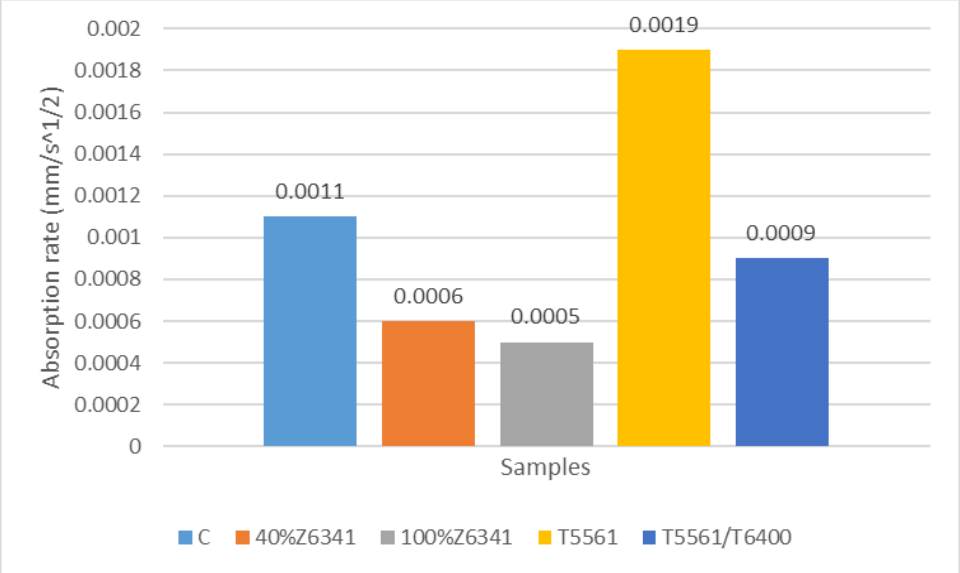

Figure 37: Secondary rate of absorption - Mix design 0.42

By comparing each mix design apart, the initial rate of absorption of the control specimen was higher than the initial rate of all the other specimens. The specimens treated with silane either diluted or not, showed a low rate of water absorption. The result is an indicator that the organic treatment decreases the amount of water sucked in the concrete pores. Moreover, the post treatment (TRANSIL 6400) shows an efficiency in reducing the water absorption. It is also remarkable that the TRANSIL 5561 (inorganic surface treatment) doesn't decrease the rate of absorption. As the secondary absorption rate occurs, an increase of the absorption rate related to the treated specimens an increase of the absorption rate is noticeable and this is an indicator of the long term effect of the product applied. For the control specimens, this rate decreases since from the beginning the pores have been filled with water and the specimen is consequently saturated.

By comparing the result with the initial rate of absorption of the two control samples, the specimen with a w/c=0.48 showed a higher absorption rate than the one from the mix with w/c=0.42. Indeed, the higher the w/c ratio, the larger are the pores and the larger the absorption volume.

g) Petrographic analysis

The petrographic study was performed on 10 thin sections (2 × 4 in) (5 for each mix design and one per sample). The information was provided for each observation and related to: carbonation rate, the capillary voids, the voids and the cracks. The following tables summarize the findings.

Table 8: Petrographic analysis results for mix design w/c =0.48

Sample ID	w/c	Carbonation	Capillary pores	Voids	Cracks
C	0.48	- Sample completely carbonated	- High amount of capillary pores	- Important bleeding channels	- No information provided
40%Z6341	0.48	- Intense at the top layer -Isolated and relatively low	- Normal distribution	- No voids at the surface	- Normal micro-cracks
100%Z6341	0.48	- Same as sample 40%Z6341	- Normal distribution	- Low voids distribution	- Some vertical cracks.
T5561/PLUS	0.48	- Intense at the surface but going deeper	- Some capillary pore.	- Normal voids distribution	- Normal shrinkage cracks
T5561/T6400	0.48	- Similar type as all the other samples at the top thin layer	- Low capillary pores.	- Normal entrapped voids.	- Normal micro-cracks

All figures are presented in the Appendix B.

It should be noted that all specimens cured following the same method as depicted earlier and during the same time.

Table 9: Petrographic analysis results for mix design w/c =0.42

Sample ID	w/c	Carbonation	Capillary pores	Voids	Cracks
C	0.42	-Huge carbonated	- Capillary voids relatively high	- Entrapped voids	- Cracks visible at top
40%Z6341	0.42	- low compared to the 40%Z6341(0.48)	- Normal distribution	- No voids at the surface	- Normal micro-cracks
100%Z6341	0.42	- Intense carbonation at the surface missing.	- Normal distribution	- Normal voids distribution	- No information provided
T5561/PLUS	0.42	- Normal carbonation at the top thin layer (higher than the T5661/T6400)	- Low capillary pores	- Normal entrapped voids	- Some cracks
T5561/T6400	0.42	- Intense at the top layer	- Low capillary pores and no bleeding channels.	- Normal entrapped voids.	- Normal micro-cracks

h) X-Ray fluorescence test

The X-Ray Test was performed on all the treated and untreated specimens at the top surface and at a depth of 2, 4 and 6 mm in order to identify and quantify the chemical composition of the surface treatment. Knowing the chemical composition of the surface treatments, there trace can be identified on the specimens.

According to the manufacture's information the chemical composition of the different surface treatments used for this test is summarized in the following table:

Table 10: Surface Treatments chemical composition

Surface Treatment	Chemical Composition					
TRANSIL 5561/PLUS	Si	Cl	K	As	Li	H2O
Silane 6341	Si	K	Al	Ge		H2O
TRANSIL 6400	Si	Cl	K	Ca	Ge	H2O

The results of the X-ray on the specimens are the following:

Table 11: X-Ray Results for w/c=0.48

w/c = 0.48	Ca (%)	K (%)	S (%)	Al(%)	Si(%)	Cl(%)
C	20.92	1.35	0.06	0.68	18.62	0.00
40% Z6341 surface	21.80	1.58	0.04	1.00	15.88	0.00
40% Z6341 Average	23.18	0.83	0.79	0.78	21.55	0.02
100%Z6341 surface	18.98	1.58	0.04	0.74	21.88	0.00
100%Z6341 Average	23.74	0.93	0.75	1.00	20.95	0.02
T5561/PLUS Surface	18.98	1.58	0.04	0.74	21.88	0.00
T5561/PLUS Average	21.36	0.79	0.82	0.81	21.58	0.01
T5561/T6400 surface	17.56	1.67	0.00	0.61	22.59	0.00
T5561/T6400 average	23.14	0.82	0.68	0.79	22.64	0.00

Table 12: X-Ray Results for w/c=0.42

Sample 0.42	Ca (%)	K (%)	S (%)	Al(%)	Si(%)	Cl(%)
C	22.22	1.41	0.04	0.64	16.34	0.00
40% Z6341 surface	22.57	1.45	0.04	0.62	13.60	0.00
40% Z6341 Average	19.50	1.02	0.75	0.76	24.43	0.02
100%Z6341 surface	21.59	1.49	0.04	0.56	13.89	0.00
100%Z6341 Average	20.85	1.28	0.65	0.89	22.96	0.01
T5561/PLUS Surface	18.52	1.75	0.04	0.55	24.96	0.02
T5561/PLUS Average	20.58	0.99	0.71	0.65	21.22	0.01
T5561/T6400 surface	18.46	1.58	0.04	0.59	22.32	0.01
T5561/T6400 average	20.89	1.07	0.58	0.92	23.91	0.01

The “Average” value represents the percentage average of each chemical element between 2 to 6mm depth. The X-Ray gun was not able to identify the lithium since it is a light element. Since the Si and S are also present in the mortar due to the sand, no valuable results can be interpreted using the data provided by the XRF.

i) Rapid chloride penetration test

This test method is based on measuring the electric conductivity through the specimen as a mean to determine the permeability of the chloride ions as a function of time. The more permeable the concrete is, the more chloride ions will migrate through the specimen, and a higher current will be measured by a device connected to it. The test was conducted for 6 hours after the specimens were soaked in water for 24 hours. The PROOVE'it system applies an electrical potential across the test in accordance to the ASTM C 1202 and will give a direct measurement of the current.

The test was performed on the 5 specimens for each mix design (w/c = 0.48 and 0.42) and the results are depicted in Appendix C. It is noted that the blue line designates the evolution of the heat during the 6 hours' test.

For each mix design, according to the results obtained, the untreated specimen showed a high penetration to chloride ions. By comparing the Transil 5561/PLUS and the Transil 5561/PLUS and TRANSIL 6400, the T5561/T6400 showed a lower permeability for the two mix designs. The permeability of the chloride ions is significantly lowered when using the Silane Z6341. The higher the percentage of silane, the better resistance to chloride penetration. In general, it has been shown that the lower the w/c ratio is the more resistant the specimen to chloride penetration will be.

Following the test, the specimens were transversely cut and a solution a silver nitrate $AgNO_3$ was added to identify the presence of chloride ions in the specimen (Figure 38). The intensity of the change of color is an indicator of the intensity of the chloride ions in the specimen.

Figure 38: Identification of chloride ions in the specimens

2. Analysis of the results

The data of the variation of the cumulative mass loss of the specimen treated with Silane Z-6341 was used to determine the fitting curve by using a regression analysis and SOLVER on Excel (Figure 32). The equation of the variation of the mass loss as a function of the number of cycles is:

$$m = e^{[\ln(x_0) - \left(\frac{A}{N}\right)^{\alpha}]} \quad (2)$$

Where,

m = cumulative mass loss

N = Number of cycles

x_0 , A and α are fitting coefficient.

In this section of this project, the efficiency of organic surface treatments as Silane and inorganic products as Transil was studied regarding abrasion and freeze/thaw cycles tested on mortar specimens to avoid the impact of the aggregate properties on the results. It has been shown that the organic surface treatments have a poor effect on increasing the wear resistance of the surface. In opposition, the inorganic surface treatments showed a significant improvement of the surface resistance to wear. Regarding the salt scaling test, the organic surface treatments performed well compared to the inorganic ones. It has been shown too that the use of a post surface treatment such as the TRANSIL 6400 in this case can improve the properties of inorganic surface treatments with respect to frost resistance. Moreover, tests showed that the abrasion test has little effect on the surface treatments used since the resistance to frost damage is still remarkable after the specimens have been abraded.

In addition, by analyzing the results from the mortar mix design (Mix 5) with a w/c= 0.48, it was demonstrated that the Silane (40%Z6341 and 100%Z6341) and the Transil 5561/PLUS with the TRANSIL 6400 decrease the carbonation with depth even though this carbonation is present at the surface. By comparing the efficiency of the TRANSIL 5561/PLUS and T5561/T6400, the post treatment decreased the carbonation rate. In addition, important amount of capillary pores and voids were identified in the control sample. No voids were found at the surface of the specimens treated with Silane.

Regarding the results obtained from the mix design (Mix 6) with w/c = 0.42, the carbonation is still important in the whole untreated specimen. According to the results from the other samples, the same conclusions can be made. As the water to cement ratio

decreases, the carbonation rate decreases by comparing the carbonation of the specimen treated with 40% Silane for the mix design with w/c=0.48 and w/c=0.42.

CHAPTER V

AN APPROACH TO CHARACTERIZE THE WEARABILITY OF CONCRETE PAVEMENT SURFACE TREATMENTS [3]

The following method can be used as an approach to predict the concrete pavement's life under dry erosion damage regardless of the type of abrasion test used to evaluate the efficiency of a surface treatment.

1. Analytical approach

During the abrasion test, the abrading cutter generated a circular wear path on the concrete surface. An effective shear stress term, τ, is proposed to quantify the average stress level on the abrading zone of concrete specimen (Figure 39). This shear stress will evoke a mass loss gradually resulting to a wear depth.

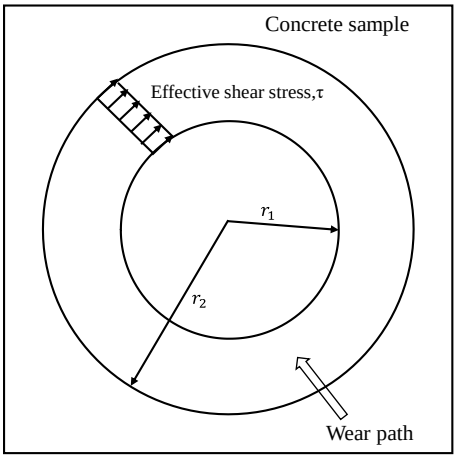

Figure 39: Effective shear stress

[3] Part of the contents in this chapter is reprinted with permission from:
An approach to characterize the wearability of concrete pavement surface treatments, by Abou Sleiman C., Shi X., and Zollinger D., Transportation Research Record: Journal of the Transportation Research Board, 2019. DOI: https://doi.org/10.1177/0361198118821668.

The averaged abrasion depth, D, is computed:

$$D = \frac{\Delta V}{A} \quad (3)$$

ΔV= Volume of material loss during the test (m^3),

$$\Delta V = \frac{\Delta m}{\rho} \quad (4)$$

Δm = mass loss.

A = cutter contact area (m^2), which equals to the area of wear path.

ρ = density of concrete.

A term, the abrasion coefficient (c), is further defined to account for the velocity of the abrading surface. This coefficient is then converted to a dimensionless term using the depth of wear.

$$c = \frac{D}{vt} \quad (5)$$

V = $200\text{rpm} = 0.9299\text{m/s}$ = The velocity of the abrading cutter (m/s)

T = $6\ \text{minutes} = 360\ \text{s}$ = test time (s)

Table 13 summarizes the results for each mix obtained during the abrasion of the specimens from Mix 1&2.

Table 13: Abrasion coefficient and Averaged depth of wear

Mix design	Specimen Type	ID	ΔV (m^3) × 10^{-6}	D (m)	Abrasion coefficient × 10^{-7}
River Gravel	Control	$C_{N/F}$	2.78	0.000488	14.56
	Treated Specimens	$T1_{N/F}$	2.34	0.000410	12.25
		$T2_{N/F}$	2.45	0.000429	12.82
Limestone	Control	$C_{N/F}$	1.72	0.000302	9.02
	Treated Specimens	$T1_{N/F}$	1.89	0.000332	9.91
		$T2_{N/F}$	1.89	0.000332	9.91

The abrasion coefficient can also be determined using its relationship with the strength of the material and the shear stresses induced by the tire. A large abrasion coefficient implies a more abraded surface since the average abrasion depth D is important. The stress/strength, R, of the concrete is obtained:

$$R = \frac{\tau}{f_\tau} \quad (6)$$

Where, f_τ = the shear strength of the material and τ = the shear stress.

It is assumed that the relationship between the abrasion coefficient, c, and the stress/strength, R, can be correlated linearly as (X., 2019):

$$c = mR + n \quad (7)$$

Where m and n are fitting coefficients.

The value R can be determined knowing the shear stress on the pavement and the shear strength of the material. Following that, the linearity between R and the abrasion coefficient, c, will lead to determine the exact value of this abrasion coefficient.

The allowable abrasion coefficient is given by:

$$c(R) = \frac{D_f}{vt} \quad (8)$$

D_f = The allowable abrasion depth.

V =The traffic speed.

T = The traffic load application time.

The allowable number of load repetitions N_f can be expressed as a function of the traffic speed, time and pavement's texture wavelength λ. An increase in the texture wavelength is an indicator of an increase in roughness.

The following equation can simulate the allowable number of load repetitions:

$$N_f = \frac{vt}{\lambda}\beta \quad (9)$$

Where β is a fitting coefficient and λ is the texture wavelength.

Therefore,

$$N_f = \frac{D_f}{c(R) * \lambda}\beta \quad (10)$$

This model is limited to a specific range of pavement textures, λ (i.e. values between 1 to 10 mm). The imposed range of λ prevents a bad rolling resistance ($\lambda \geq 10$ mm), ride quality ($\lambda \geq 100$mm), vehicle wear ($100\ mm \leq \lambda \leq 5$ m), and tire wear ($1\ \mu m \leq \lambda \leq 1$ mm).

2. Load Stresses

As it was stated earlier, the number of load repetitions is a function of the abrasion coefficient. This coefficient is determined according to the magnitude of the shear stresses applied on the specimen and depends on the nature of the load.

From the torque generated in the abrasion testing, the shear stress can be determined as follow:

$$T = \int_{r_1}^{r_2} 2\tau\pi r^2 dr \tag{11}$$

Upon rearrangement, this expression yields:

$$\tau = \frac{3T}{2\pi(r_2^3 - r_1^3)} \tag{12}$$

Where,

r_1 = inner radius of the wear path

r_2 = outer radius of the wear path

The shear stresses under a moving truck tire exist in both transverse and longitudinal directions. In order to adopt the proposed model, the magnitude of the shear stresses must be determined. In a study by Tielking and Abraham (Tielking, 1994) a load pin array developed by the Precision Measurement Company of Ann Arbor, Michigan was used to measure the tire-pavement shear pressures (Figure 40 - 41). The load pin signal would respond to dynamic tire contact pressure.

The study was focused on measuring the footprint pressures in order to accurately predict pavement damage.

Figure 40: Wire based tire - Reprinted from (Tielking, 1994)

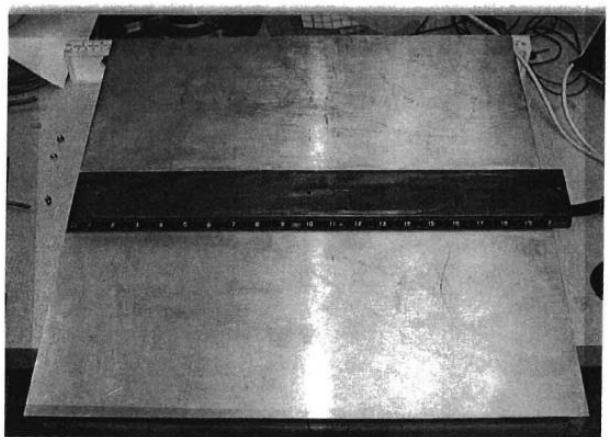

Figure 41: Contact plate and load pin array - Reprinted from (Tielking, 1994)

3. Field Data

The skid resistance is defined as the force developed when a tire is prevented from rotating along the pavement surface. This parameter changes over time and depends on a pavement surface's microtexture and macrotexture and thus is related to the texture wavelength (Hou, 2018). The larger λ is, the greater the loss of skid resistance will be. At the same time, it is not preferable to have a very low texture wavelength (microtexture) even though the grip of the tire will be important since it will affect the tire wear. The shotblasting method has been used to increase the skid resistance but it was demonstrated that a chemical densifier lithium silicate is more advantageous when the chemical is applied to porous pavement surface. In a 3-year study by the Oklahoma Department of

Transportation, a section of concrete pavement on State Highway 77 consisted of a "densifier-over-shotblasting" (DOS). The field tests included different pavement preservation treatments. The average daily traffic on the road tested was around 14,000 vehicles. The study took monthly measurements of skid numbers for 33 months (Riemer, 2012).

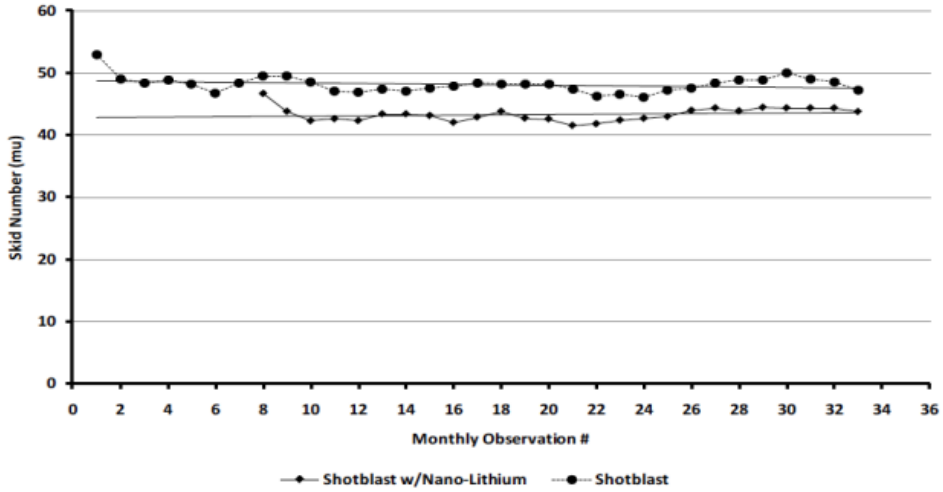

Figure 42: Oklahoma DOT Study Results of Skid Number Change over Time - Reprinted from (Haworth, 2011)

According to figure 42, the DOS section retained its skid number for 26 months at an average of 44 (Haworth, 2011).

Another field study by Haworth (Haworth, 2011), sponsored by California's Department of Transportation, CALTRANS, was conducted on a test site on Interstate Highway 80 over Donner Pass in the Sierra Mountains. The study evaluated DOS applied to rigid pavements and determined the surface wear over 12 months. For a shotblasted surface, the wear depth was equal to 5.29 mm compared to 2.12 mm for a DOS. It was concluded that the lithium silicate densifier over shotblasting treated specimens have about half the wear of untreated section.

4. Determination of the fitting coefficient β

Abrasion related performance can be calibrated from the above model using the field results obtained by Haworth.

In general,

$$N_i = \frac{D_i}{c(R) * \lambda} \beta \tag{13}$$

The fitting coefficient β can be determined according to the following method:

$$D = \left(c(R) * \frac{\lambda}{\beta} \right) * N \tag{14}$$

Further studies are warranted to determine the relationship between the abrasion depth and the number of load repetitions. To simplify the approach, this relationship is considered linear and thus $\left(c(R) * \frac{\lambda}{\beta} \right)$ is the slope of the line, D and N are the two variables.

The value of β can be calculated by determining the slope of the line and calculating the abrasion coefficient according to the shear stress induced by the tires (De Beer, 1997). The value of the texture wavelength can be established from field measurements using a laser-based profilometry.

The equivalent single axle load (ESAL) can be considered as a damage factor to characterize the number of load repetitions based on, for instance, the AASHTO Road Test equivalency tables. In case of the Interstate Highway 80, the average daily traffic is considered equal to 25,000 which leads to an ESAL of 395,569. This value is not a precise one due to the lack of data at the time of the test. After 12 months, the wear depth recorded

is equal to 2.12mm using the densifier-over-shotblasting method according to the Caltrans Study. More data is required to draw the actual evolution of the depth wear as a function of the shear stress associated with the applied wheel load. Following this, either the fitting coefficient β or any number of load repetitions in regard of a specific designated allowable depth of wear can be determined. Figure 43 shows the variation of the depth of wear as a function of the number of ESALs.

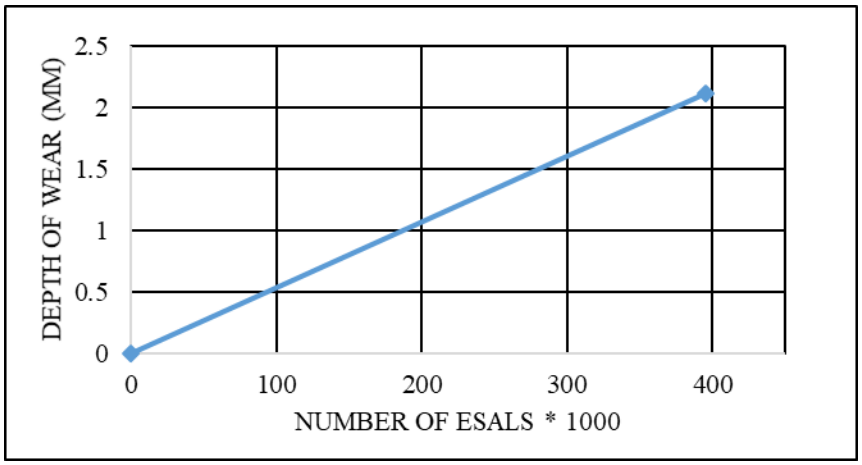

Figure 43: Evolution of the depth of wear with the number of ESALs

The approach to predict the allowable number of load repetitions is related to two parameters: The abrasion coefficient which is a function of the material mass loss due to the abrasion test and the pavement's texture wavelength. The abrasion coefficient can be determined using the assumed linearity between this coefficient and the stress/strength ratio according to the magnitude of the shear stress induced on the pavement by the tires. From the field results obtained by Oklahoma DOT, it was demonstrated that the surface treatment applied helped maintaining a skid number over 26 months. In addition, the surface treatment significantly reduced the wear depth after 12 months according to the

referenced Caltrans study. The data collected can be used to calibrate the β coefficient by relating it to the number of allowable repetitions. Applying this model to the surface treatment used, it was deduced that the allowable number of load repetitions increased by 14%.

The concrete pavement life can be predicted by following the steps as below:

1. Execute the abrasion test according to the ASTM standards.
2. Develop the correlation between the abrasion coefficient, c, and the stress/strength, R using the testing data.
3. Numerically compute the induced stress/strength R_j for the traffic load classification j.
4. Determine the abrasion coefficient c.
5. Determine the value of the texture wavelength using a laser-based profilometry.
6. Set an allowable depth of wear and calculate consequently the allowable number of load repetitions.

CHAPTER VI

SUMMARY AND CONCLUSIONS

In this study, the results from the laboratory testing depict the efficiency of specific chemical surface treatments regarding durability of a concrete pavement surface. Even though the ASTM test procedures were not fully executed, the common thread of porosity that passed through the test results attest to their validity with respect to resistance to abrasion, impact, freeze/thaw cycles, and permeability. Consequently, all the test results are related and are useful to either justify or support the results of the other testing to be carried out beyond this study. For instance, the abrasion resistance of the surface is related to the strength of the concrete and also to the porosity of the surface (which was varied by changing the w/cm of the prepared mixtures). The freeze/thaw resistance is associated to the size of the pores in the concrete matrix and the size of the aggregates used. Furthermore, the results are well distinctive with regard to the nature of the surface treatments whether they were organic such as silane or inorganic such as lithium.

Part of this study showed that the use of an inorganic surface treatment (such as TRANSIL®5561/PLUS) increases the resistance to abrasion and freeze/thaw cycles. This resistance was also attributed to the compressive strength of the mix as well as the type of aggregates used. The test results indicated a positive correlation between an increase in the resistance to abrasion with an increase of the concrete compressive strength. The role of aggregate size was manifest by lower resistance to freeze/thaw damage with an increase in size. From this phase of work, it was evident that the use of an inorganic surface

treatment resulted in the increase in abrasion and freeze/thaw resistance due to a change in the porosity of the specimen.

To isolate the effect of aggregates on abrasion and freeze/thaw durability, the second phase of testing consisted of preparing abrasion and freeze/thaw mortar specimens treated with inorganic and organic surface treatments. Test results showed a lower cumulative mass loss which also assert a change of porosity of the concrete surface due to the treatments. The specimens treated with organic products did not show any mass loss.
In order to further identify the effect of porosity on performance, several laboratory tests were performed including the water sorptivity, chloride penetration and petrographic analysis. The petrographic analysis showed lower capillary-sized porosity for specimens treated with inorganic surface treatments (such as TRANSIL 5561/T6400, TRANSIL 5561). While specimens treated with organic products (such as Silane Z 6341 and Silane Z 6595), manifest a greater amount of capillary porosity. These observations were further validated from water sorptivity and chloride penetration tests of inorganic and organic treatments where a reduction in the ingress of water and chloride ions was the result. Better results related to the specimens treated with organic products were obtained.

The tests result also revealed the mechanism of how organic and inorganic surface treatments affect the surface porosity which dictates resistance to abrasion and freeze/thaw damage. Inorganic products decrease the size of the pores by reacting with the lime at the surface and organic treatments consist of small particles which enter the pores of the concrete matrix to form a water repellent lining on the pore walls without changing the size of the pores.

Finally, a mathematical approach was elaborated in order to predict the life of a pavement under dry erosion due to traffic. This approach is a function of the allowable number of load repetitions, the abrasion coefficient and a limited range of a pavement's surface texture wavelength. This model predicts for inorganic surface treatments that the allowable number of load repetitions increased by 14%. In addition, the model can be used by the transportation community to predict the service-life of a concrete pavement surface based on material and traffic characteristics.

The limitations of this test program organized in this thesis along with the future studies are depicted in Appendix D.

REFERENCES

ACI.2R-01. (2001). *Guide to Durable Concrete, ACI manual of concrete Practice, Part 1, ACI Committee 201*. Farmington Hills, MI: American Concrete Institute.

Bentz, D. P., Ehlen, M. A., Ferraris, C. F., & Garboczi, E. J. (2001). Sorptivity-based service life predictions for concrete pavements. *National Institute of Standards and Technology*, 181-193.

Bertolini, L., Elsener, B., Pedeferri, P., Redaelli, E., & Polder, R. (2013). Corrosion of steel in concrete: Prevention, diagnosis, repair, Wiley, Chichester, U.K.

Cossale, G., Elliott, R., & Widyatmoko, I. (2013). The Importance of Road Surface Texture in Active Road Safety Design and Assessment. *Road Safety and Simulation International Conference.* Rome, Italy.

Costa, A., & Appleton, J. (1999). Chloride penetration into concrete in marine environment - Part I: Main parameters affecting chloride penetration. *Materials and Structures*, Vol 32, pp 252-259.

Dang, Y., Xie, N., Kessel, A., McVey, E., Pace, A., & Shi, X. (2014). Accelerated Laboratory Evaluation of Surface Treatments for Protecting Concrete Bridge Decks fro Salt Scaling. In *Construction and Building Materials* (pp. Vool. 55, pp. 128-135).

De Beer, M. C. (1997). Determination of Pneumatic Tyre/Pavement Interface Contact Stresses under Moving Loads and Some Effects on Pavements with Thin Asphalt Surfacing Layers. *8th International Conference on Asphalt Pavements (8th ICAP'97)*, (pp. 179-227). Seattle, WA.

Elsalamawy, M., Mohamed, A., & Abosen, A. (2017). Effectiveness of Crystallization Coating Materials on Chloride Ions Ingress in Concrete. *World Academy of Science, Engineering and Technology International Journal of Civil and Environmental Engineering*, Vol 11, No. 9.

French, W. (1991). Concrete Petrography: a review. *Quarterly Journal of Engineering Geology*, 17-48.

Gao, X. J., Deng, H. W., & Yang, Y. Z. (2011). Influence of Silane Treatment on the Freeze-Thaw Resistance of Concrete. In *Advanced Materials Research* (pp. Vol. 250, pp. 565-568).

Garcia, A., Castro-Fresno, D., Polanco, J. A., & Thomas, C. (2012). Abrasive Wear Evolution in Concrete Pavements. In *Road Materials and Pavement Design* (pp. Vol. 13, No. 3, pp. 534-548).

Georgali, B., & Tsakiridis, P. E. (2005). Microstruture of fire-damaged concrete. A case study. *Cement & Concrete Composites*, 255-259.

Harnik, A., Meier, U., & Rosli, A. (1980). Combined Influence of Freezing and Deicing Salt on Concrete - Physical Aspects. In a. G. P. J. Sereda, *Durability of Building Materials and Components* (pp. 474-484). West Conshohocken, PA: ASTM STP 691, American Society for Testing Materials.

Haworth, M. (2011). *Interstate 80 Donner Summit Shotblasting and Transil Application.* Oklahoma City, OK: Blastrac, Inc.,.

Hilsdorf, H., & Kropp, J. (1995). *Performance criteria for concrete durability.* Taylor & Francis, RILEM Report 12.

Horszczaruk, E. (2004). The Model of Abrasive Wear of Concrete in Hydraulic Structures . In *Wear* (pp. Vol. 256, No. 7-8, pp. 787-796).

Hou, S. X. (2018). Evaluation of Rutting and Friction Resistance of Hot Mix Asphalt Concrete using Innovative Vertically Loaded Wheel Tester. *Construction and Building Materials*, Vol. 176, pp. 710-719.

I. Flores-Vivian, V. H. (2013). Self-assembling particle-siloxane coatings for superhydrophobic concrete. *ACS Applied Materials & Interfaces*.

J. Marchand, E. S. (1994). The deicer salt scaling deterioration of concrete-an overview. *ACI SP 145*, 1-46.

Jana, D. (2007). Concrete Scaling - A Critical Review. *proc., 29th Conference on Cement Microscopy, Construction Materials Consultants, Inc., and Applied Petrographic Services, Inc., Greensburg, PA.*

Keyser, J. H. (1971). Resistance of Various Types of Bituminous Concrete and Cement Concrete to Wear Studded Tires. *Transportation Research Board, Washington D.C.*

Liu, Y., Chen, X., & Xin, J. H. (2006). Super-hydrophobic surfaces from a simple coating method: A bionic nanoengineering approach. In *Nanotechnology* (pp. Vol. 17, pp. 3259-3263). Institute of Physics Publishing.

Liu, Z., & Hansen, W. (2016). Effect of hydrophobic surface treatment on freeze-thaw durability of concrete. *Cement and Concrete Composites*, 49-60.

M.C.Limbachiya, E.Marrocchino, & A.Koulouris. (2007). Chemical–mineralogical characterisation of coarse recycled concrete aggregate. *Elsevier*, 201-208.

Meck, E., & Sirivivatnanon, V. (2003). Field indicator of chloride penetration depth. *Cement and Concrete Research 33*, 1113-1117.

Mielenz, R. C. (1962). Petrography applied to Portland Cement Concrete. In T. &. Inc: Fluhr, *Reviews in Engineering Geology* (pp. 1,1 - 38). Geological Society of America, GAEGA.

Mindess, S., Young, J. F., & Darwin, D. (2002). *Concrete - Second Edition.* Pearson Education, Inc.

Otsuki, N., Nagataki, S., & Nakashita, K. (1992). Evaluation of AgNO3 solution spray method for measurement of chloride penetration into hardened cementitious matrix materials. *ACI Mater. J. 89 (6)*, 587-592.

Pan, X., Shi, Z., Shi, C., Ling, T.-C., & Li, N. (2017). A review on Concrete Surface Treatment Part 1: Types and Mechanisms. *Construction and Building Materials*, Vol. 132, pp. 578-590.

Pan, X., Shi, Z., Shi, C., Ling, T.-C., & Li, N. (2017). A review on Surface Treatment for Concrete - Part 2: Performance. *Construction and Building Materials*, Vol. 133, pp. 81-90.

Proverbio, E., & Carassiti, F. (1997). Evaluation of Chloride Content in Concrete by X-Ray Fluorescence. *Cement and Concrete Research*, Vol.27, No.8, pp. 1213-1223.

Riemer, C. D. (2012). Preservation of Concrete pavement using Modified Silicon Reactive Lithium Surface Densifier Over Shotblasting: A Life Cycle Cost Analysis. *Transportation Research Record*, Paper 12-0531.

Sabir, B. B., Wild, S., & O'Farrell, M. (1998). *A water sorptivity test for martar and concrete*. Materials and Structures/Materiaux et Construction.

Scott, B. D., & Safiuddin, M. (2015). Abrasion Resistance of Concrete-Design, Construction and Case Study. *Concrete Research Letters*, Vol. 6, No.3, pp. 136-148.

Smith, P., & Schonfeld, R. (1970-1978). Studies of Studded-Tire Damage and Performance in Ontario, Winter 1969-1970. *Transportation Research Board, Washington D.C.*

Taylor, P., Yurdakul, E., & Ceylan, H. (2012). Concrete Pavement Mixture Design and Analysis (MDA): Application of a Portable X-Ray Fluorescence Technique to Assess Concrete Mix. *InTrans Project Reports*.

Thompson, J., Silsbee, M., Gill, P., & Scheetz, B. (1997). Characterization of silicate sealers on concrete. *Cement and Concrete Research*, Vol. 27, No 10. 1561-1567.

Tielking, J. T. (1994). Measurement of Truck Tire Footprint Pressures. *Transportation Research Record: Journal of the Transportation research Board*, 1435: 92-99.

X., S. (2019). Evaluation of Portland Cement Concrete Containing Reclaimed Asphalt Pavement for Pavement Applications. *Transporation Research Record*.

Yousif, M. A.-M. (2015). Freeze-Thaw Performance of Low-Cement Content Stabilized Soils for Containment Apllications. *Dalhousie University, Halifax, NS, Canada*.

ASTM C 672. Standard Test Method for Scaling Resistance of Concrete Surfaces Exposed to Deicing Chemicals. American Society for Testing and Materials, West Conshohocken, PA, 2012.

ASTM C 1585. Standard Test Method for Measurement of Rate of Absorption of Water by Hydraulic- Cement Concretes. American Society for Testing and Materials, West Conshohocken, PA, 2011.

ASTM C 944. Standard Test Method for Abrasion Resistance of Concrete or Mortar Surfaces by Rotating-Cutter Method. American Society for Testing and Materials, West Conshohocken, PA, 2006.

ASTM C 856. Standard Practice for Petrographic Examination of Hardened Concrete. American Society for Testing and Materials, West Conshohocken, PA, 2018.

ASTM C457. Standard Test Method for Microscopical Determination of Parameters of the Air-Void System in Hardened Concrete. American Society for Testing and Materials, West Conshohocken, PA, 2016.

ASTM C 1202. Standard Test Method for Electrical Indication of Concrete's Ability to Resist Chloride Ion Penetration. American Society for Testing and Materials, West Conshohocken, PA, 2017.

ASTM C 150-07. Standard Specifications for Portland Cement. American Society for Testing and Materials, West Conshohocken, PA, 2007.

ASTM C 618. Standard Specification for Fly Ash and Raw or Calcined Natural Pozzolan for Use as Mineral Admixture in Portland Cement Concrete. American Society for Testing and Materials, West Conshohocken, PA, 2008.

ASTM C 128. Standard Test Method for Density, Relative Density (Specific Gravity), and Absorption of Fine Aggregate. American Society for Testing and Materials, West Conshohocken, PA, 2004.

ASTM C 127. Standard Test Method for Density, Relative Density (Specific Gravity), and Absorption of Coarse Aggregate. American Society for Testing and Materials, West Conshohocken, PA, 2004.

ASTM C 192. Standard Practice for Making and Curing Concrete Test Specimens in the Laboratory. American Society for Testing and Materials, West Conshohocken, PA, 2007.

ASTM C 305-14. Standard Practice for Mechanical Mixing of Hydraulic Cement Pastes and Mortars of Plastic Consistency. American Society for Testing and Materials, West Conshohocken, PA, 2014.

ASTM D 5381. Standard Guide for X-Ray Fluorescence (XRF) Spectroscopy of Pigments and Extenders. American Society for Testing and Materials, West Conshohocken, PA, 2014.

APPENDIX A: WATER SORPTIVITY RESULTS

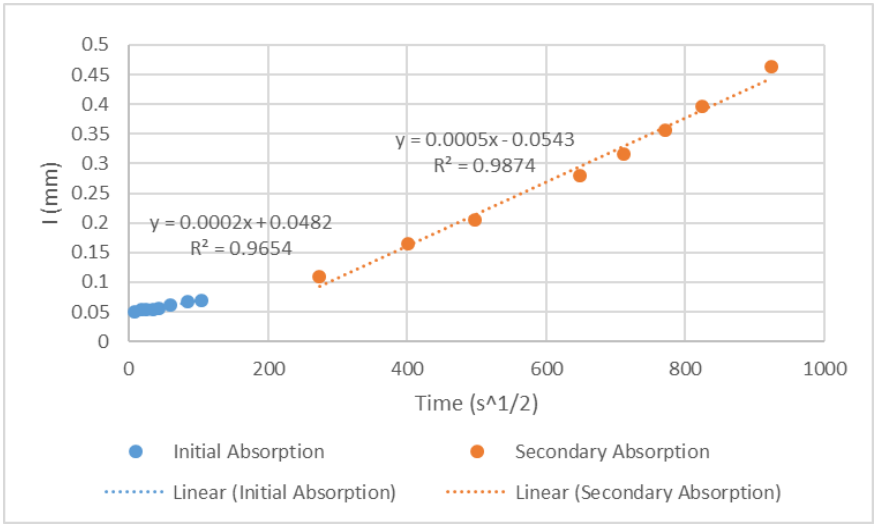

A 1: Absorption of the 40% Silane (w/c=0.48)

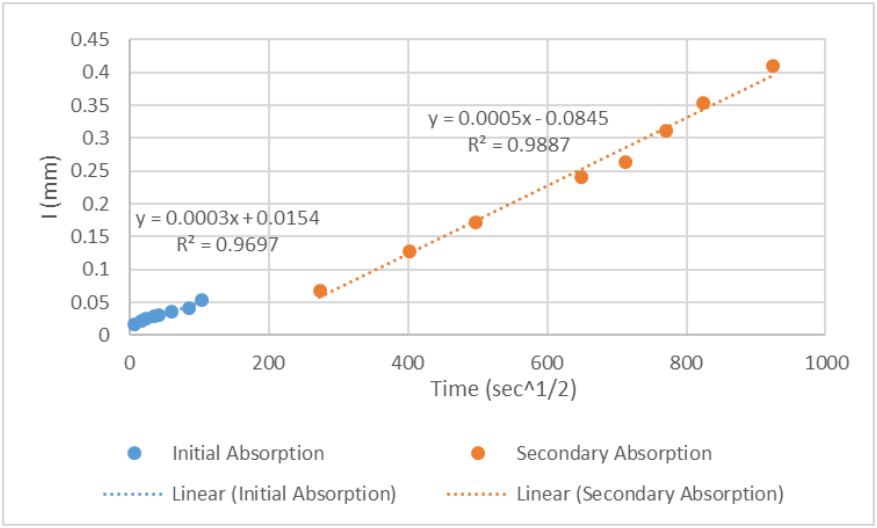

A 2: Absorption of the 100% Silane (w/c=0.48)

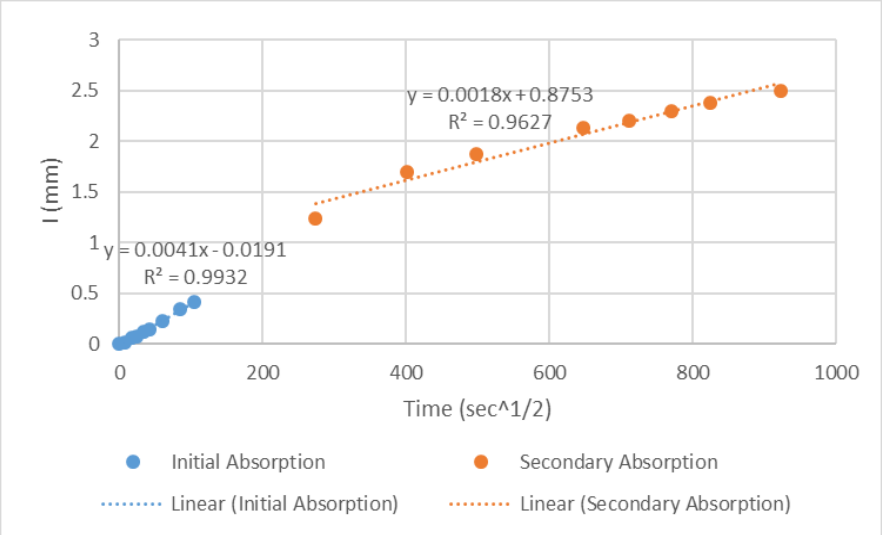

A 3: Absorption of the TRANSIL 5561/PLUS (w/c=0.48)

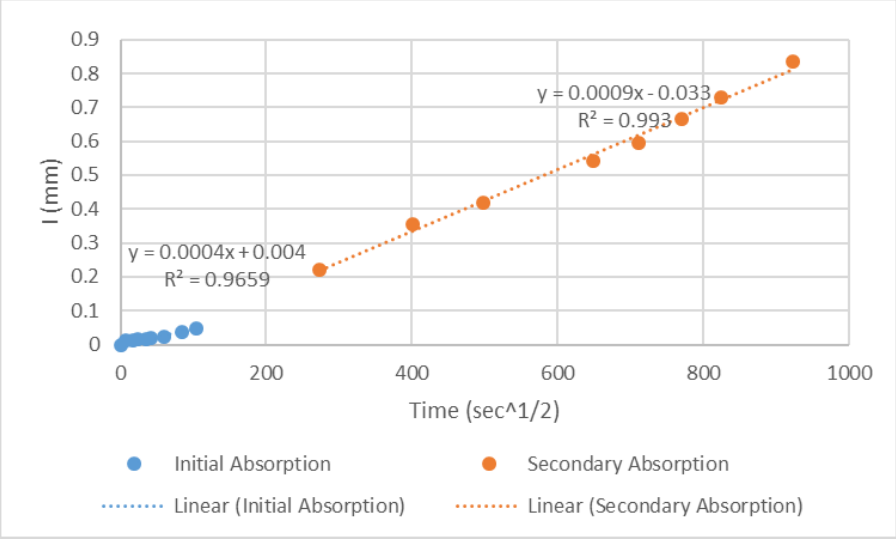

A 4: Absorption of the TRANSIL 5561/PLUS with TRANSIL 6400 (w/c=0.48)

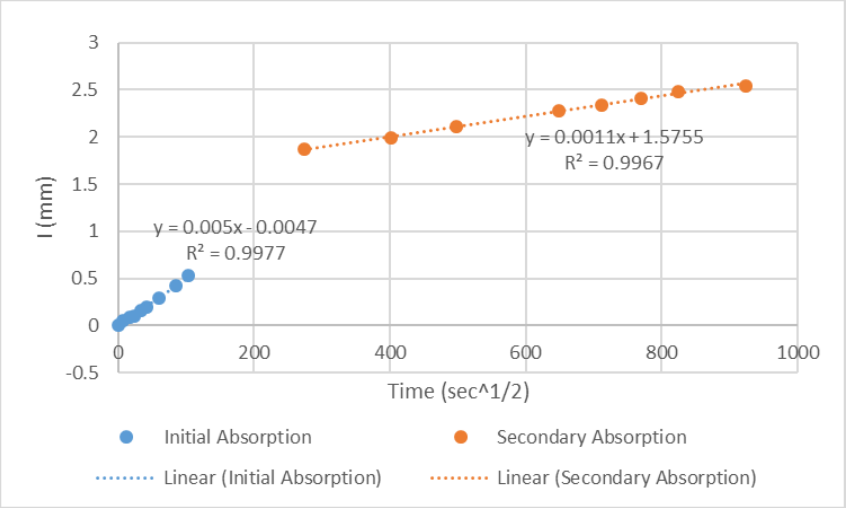

A 5: Absorption of the Control sample (w/c=0.42)

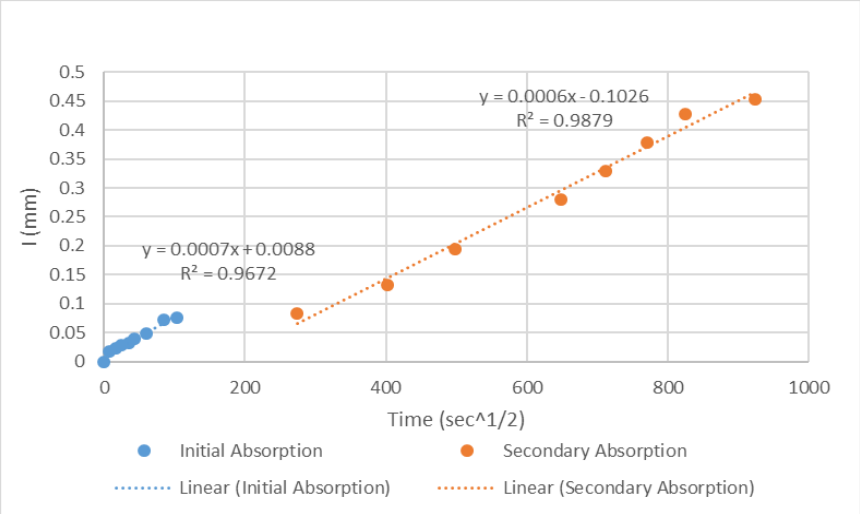

A 6: Absorption of the 40% Silane (w/c=0.42)

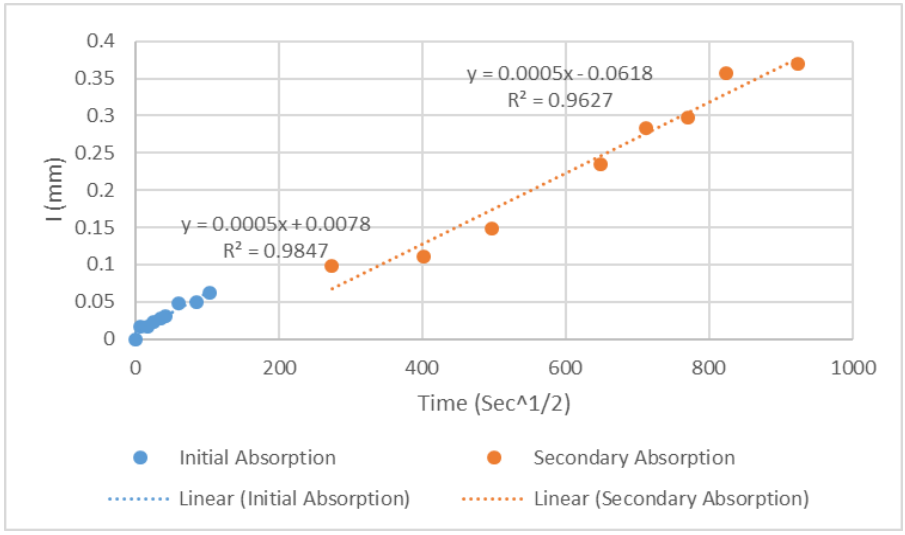

A 7: Absorption of the 100% Silane (w/c=0.42)

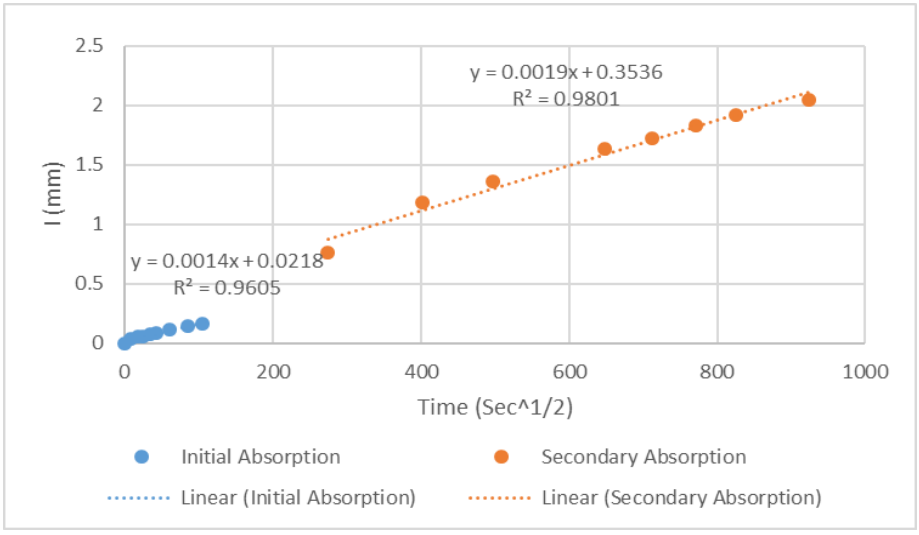

A 8: Absorption of the TRANSIL 5561/PLUS (w/c=0.42)

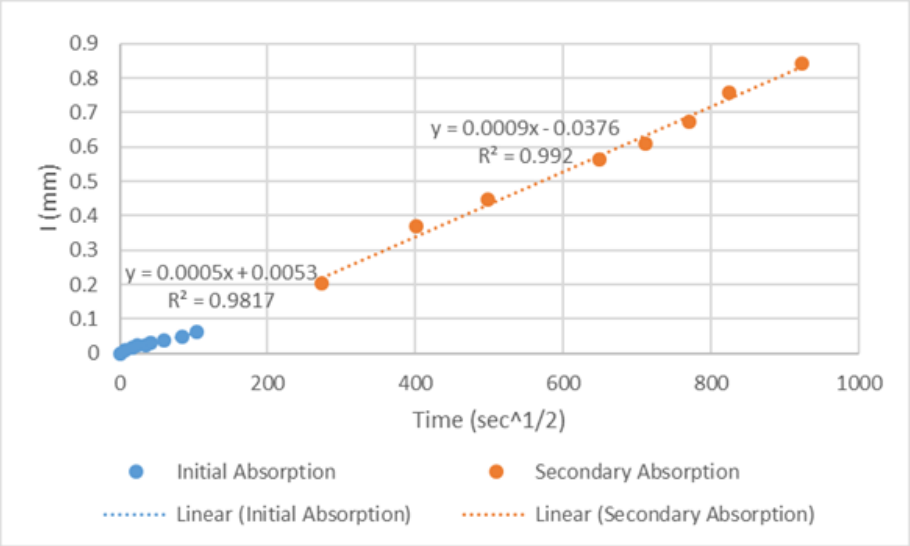

A 9: Absorption of the TRANSIL 5561/PLUS with TRANSIL 6400 (w/c=0.42)

APPENDIX B: PETROGRAPHIC ANALYSIS RESULTS

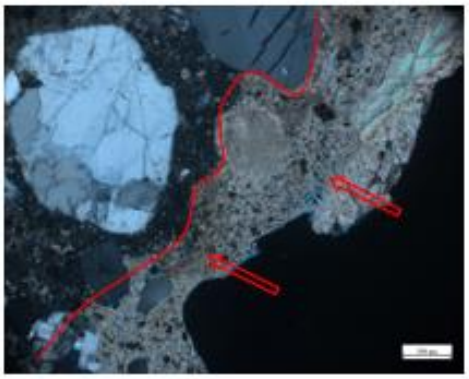

B 1: Zone carbonated_40%Z6341 0.48

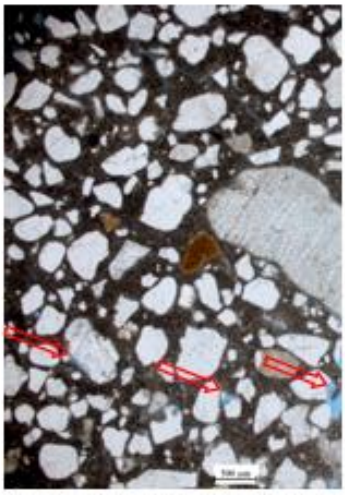

B 2: Normal distribution of voids_40%Z6341 0.48

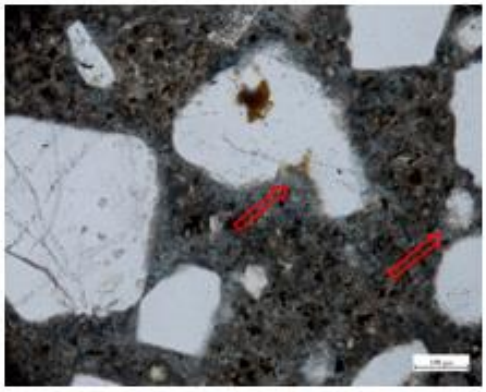

B 3: Normal distribution of capillary voids_40%Z6341 0.48

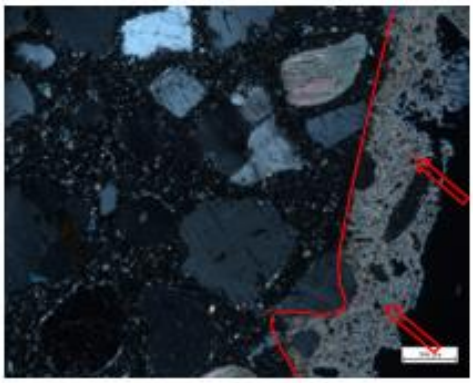

B 4: Zone carbonated_100%Z6341 0.48

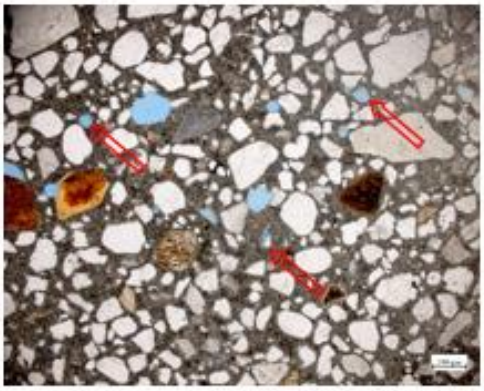

B 5: Low voids distribution_100Z6341 0.48

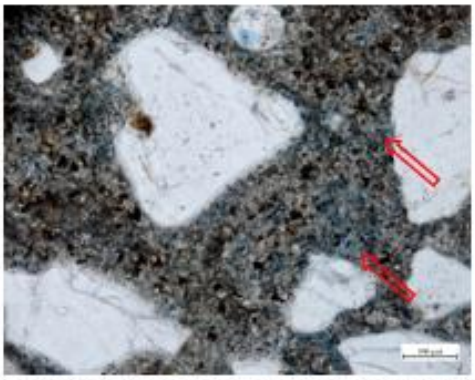

B 6: Normal capillary pores distribution_100%Z6341 0.48

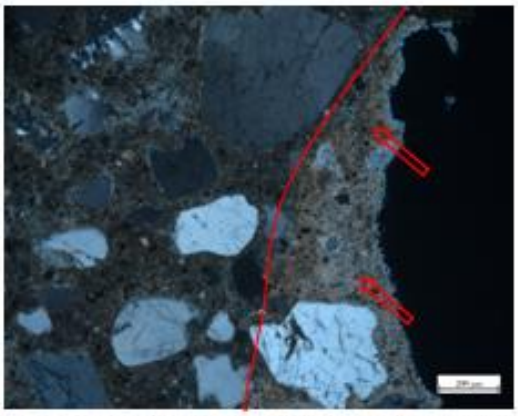

B 7: Intense carbonation at the surface_T5561/PLUS 0.48

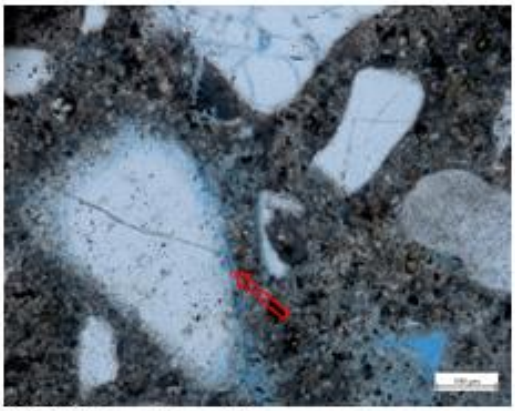

B 8: Normal capillary pores distribution_T5561/PLUS 0.48

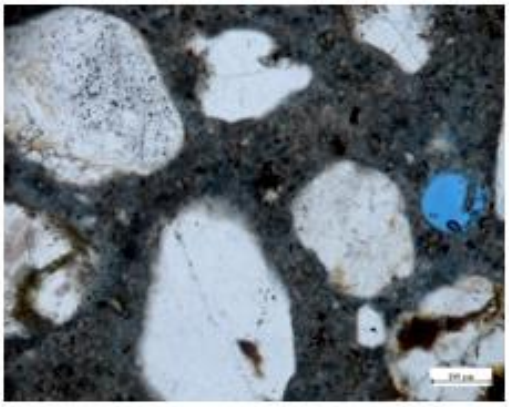

B 9: Some capillary pores_T5561/PLUS 0.48

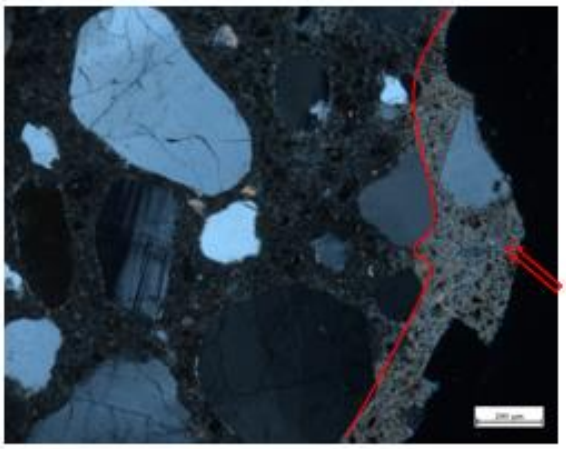

B 10: Small zone carbonated_T5561/T6400 0.48

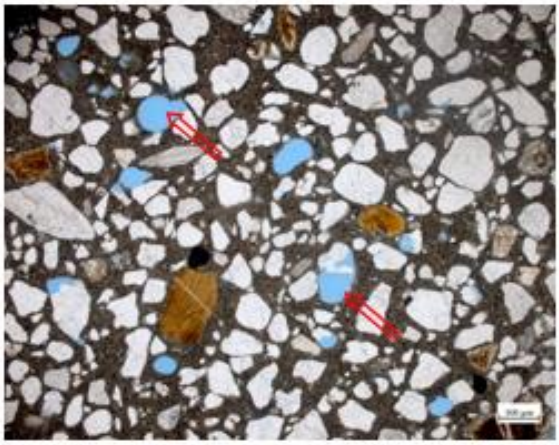

B 11: Normal entrapped voids_T5561/T6400 0.48

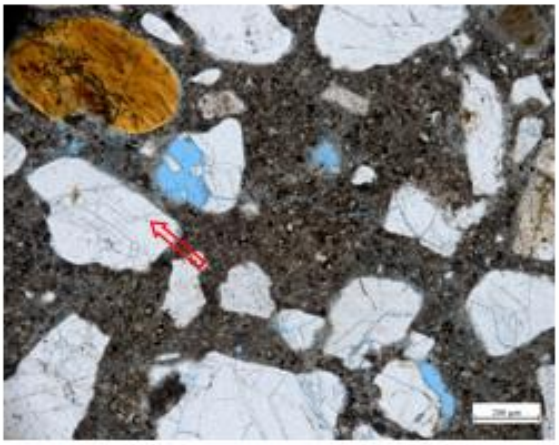

B 12: Normal shrinkage cracks_T5561/T6400 0.48

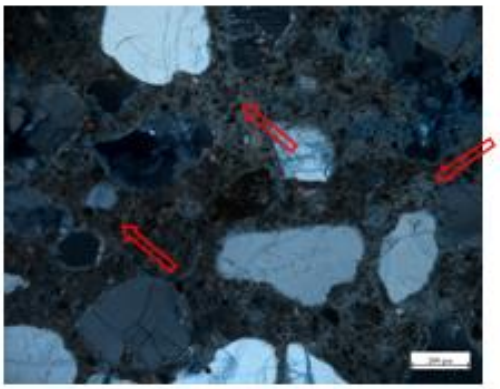

B 13: Important carbonation of the whole sample_C 0.48

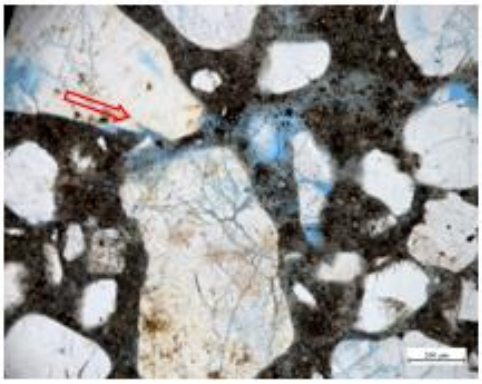

B 14: Important bleeding channels_C 0.48

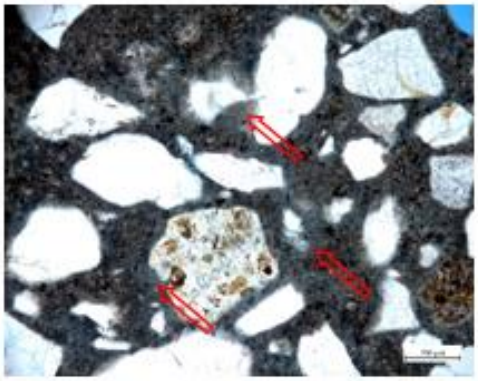

B 15: High capillary pores_C 0.48

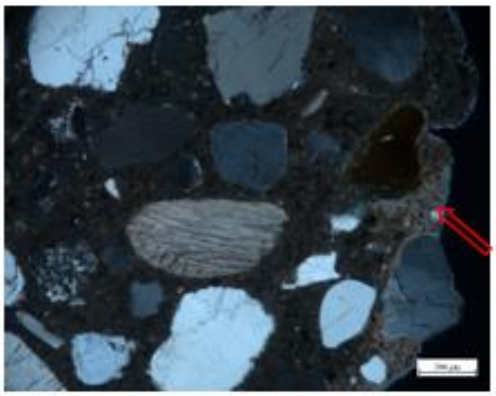

B 16: Less carbonated surface area_40%Z6341 0.42

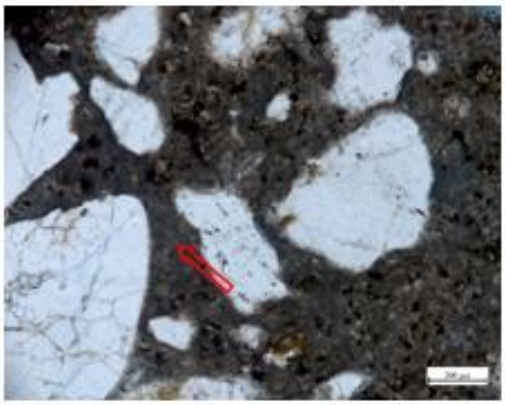

B 17: Less capillary voids_40%Z6341 0.42

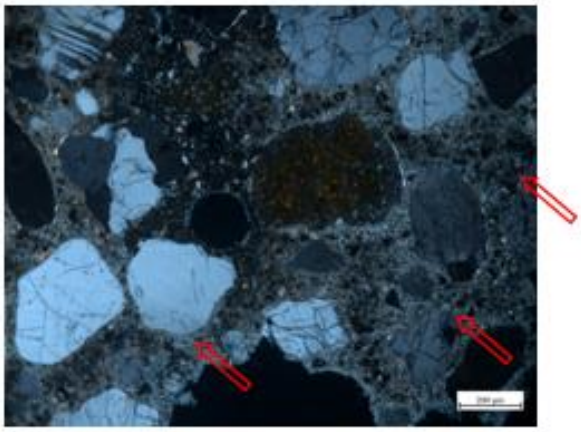

B 18: Intense carbonation at the surface missing_100%Z6341 0.42

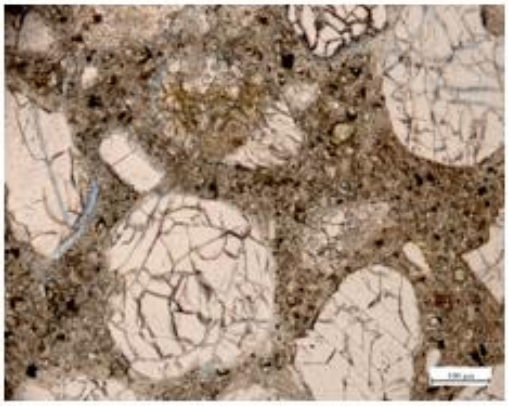

B 19: Normal capillary voids_100%Z6341 0.42

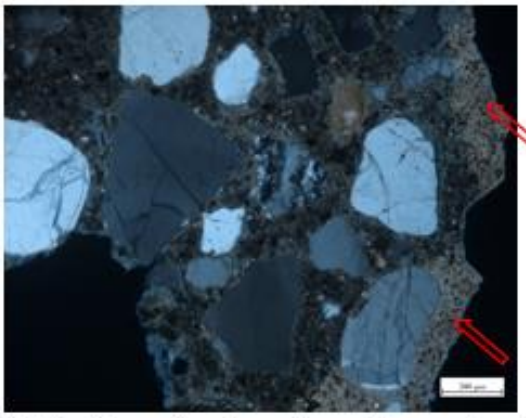

B 20: Normal carbonation at the surface but extending with depth_T5561/PLUS 0.42

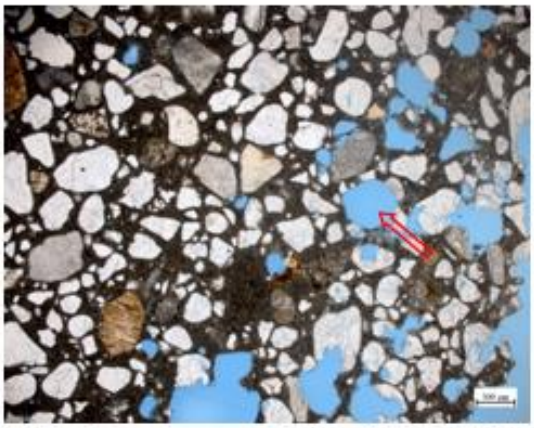

B 21: Large entrapped air voids_T5561/PLUS 0.42

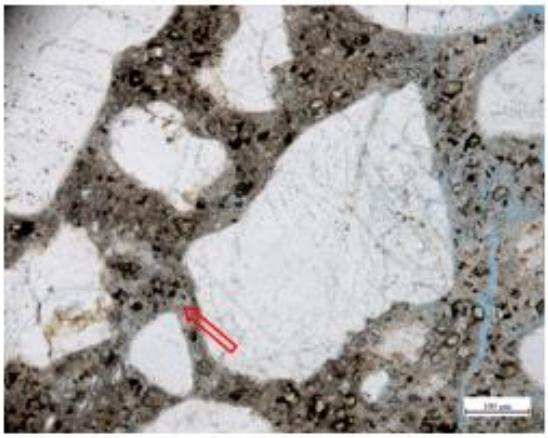

B 22: Some cracks and capillary pores_T5561/PLUS 0.42

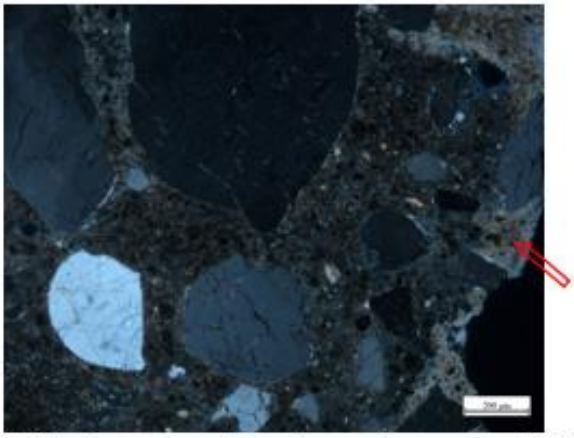

B 23: Intense carbonation at the surface_T5561/T6400 0.42

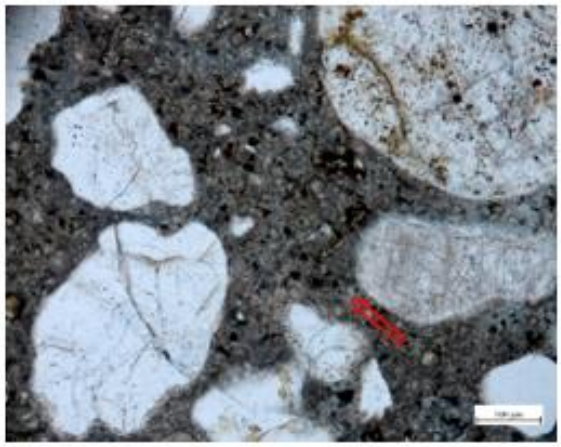

B 24: Normal capillary pores_T5561/T6400 0.42

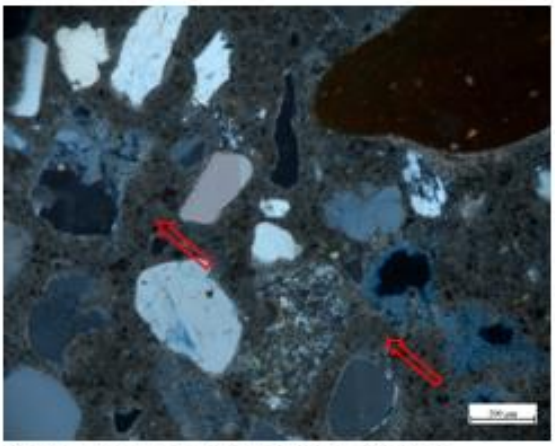

B 25: Intense carbonation_C 0.42

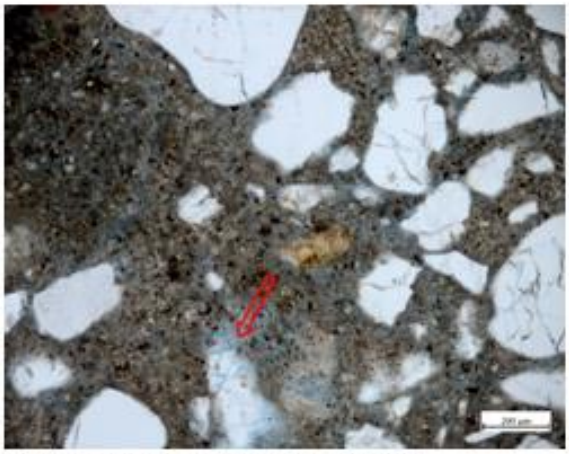

B 26: High capillary pores_C0.42

APPENDIX C: RAPID CHLORIDE PENETRATION RESULTS

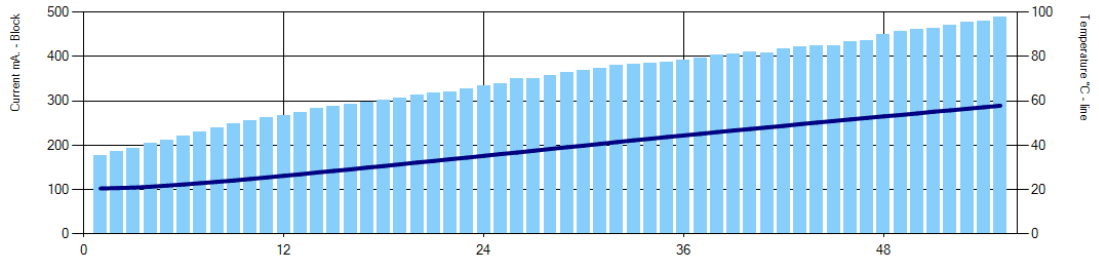

C 1: Sample C 0.48

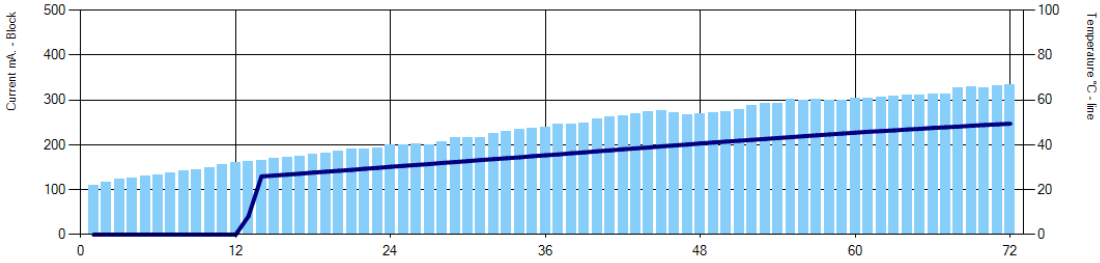

C 2: Sample TRANSIL 5561/PLUS 0.48

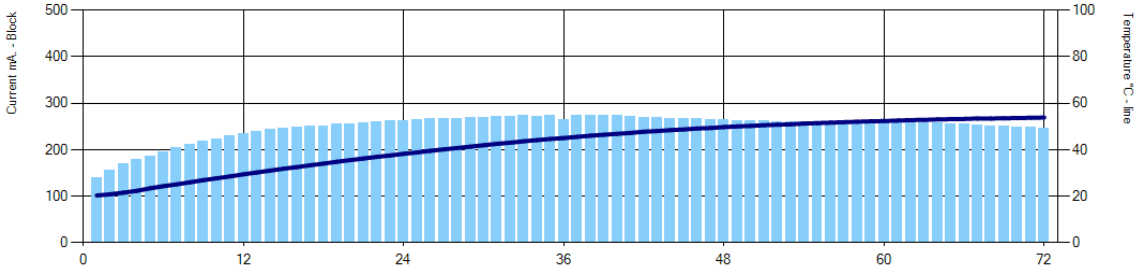

C 3: Sample TRANSIL 5661/T6400 0.48

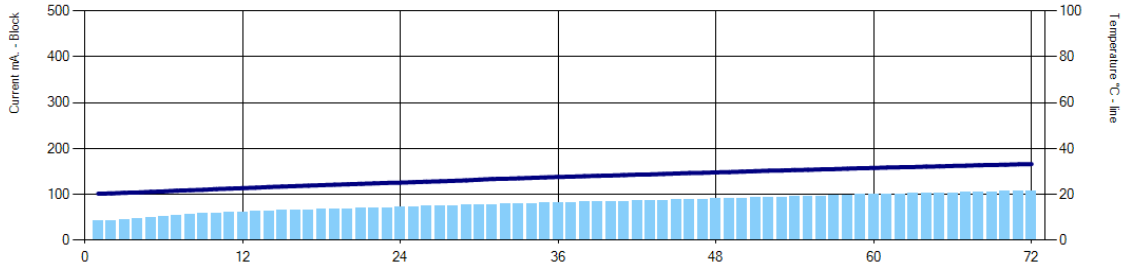

C 4: Sample 40% Z6341 0.48

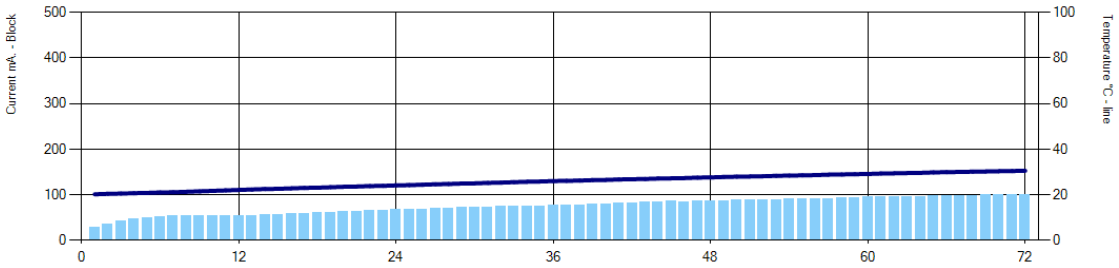

C 5: Sample 100% Z6341 0.48

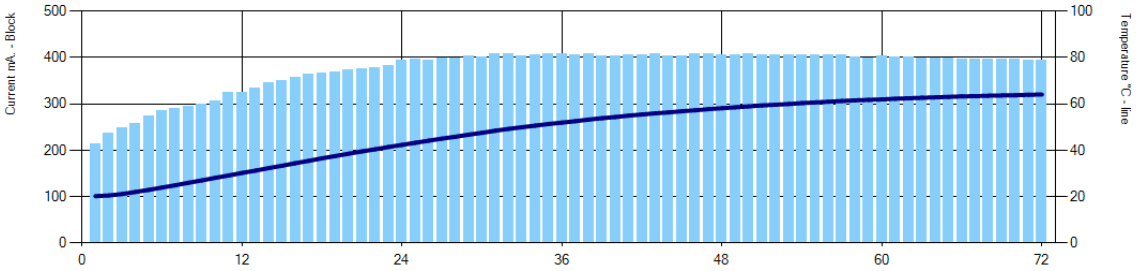

C 6: Sample C 0.42

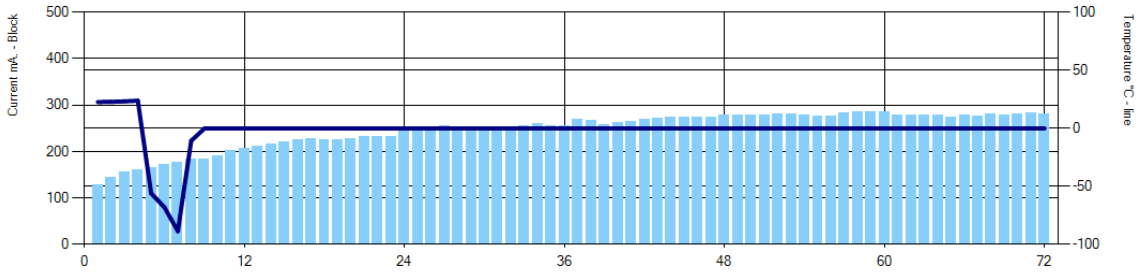

C 7: Sample TRANSIL 5561/PLUS 0.42

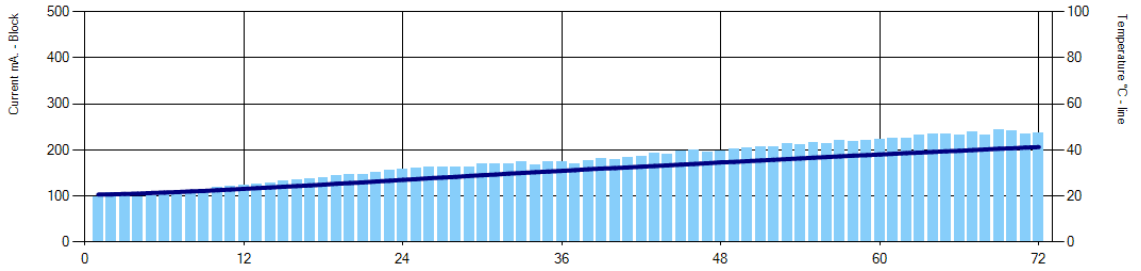

C 8: Sample TRANSIL 5661/T6400 0.42

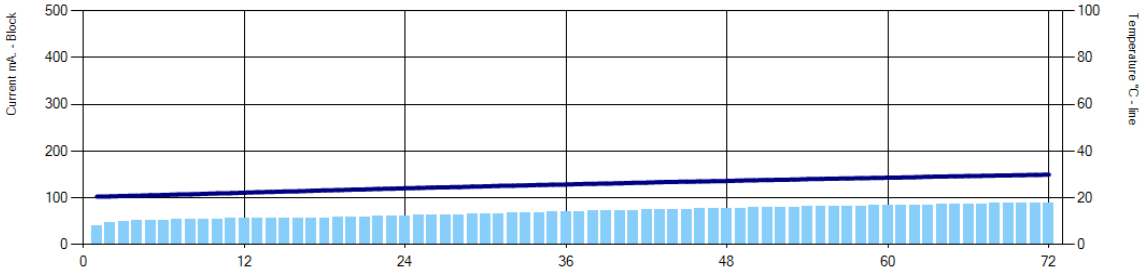

C 9: Sample 40% Z6341 0.42

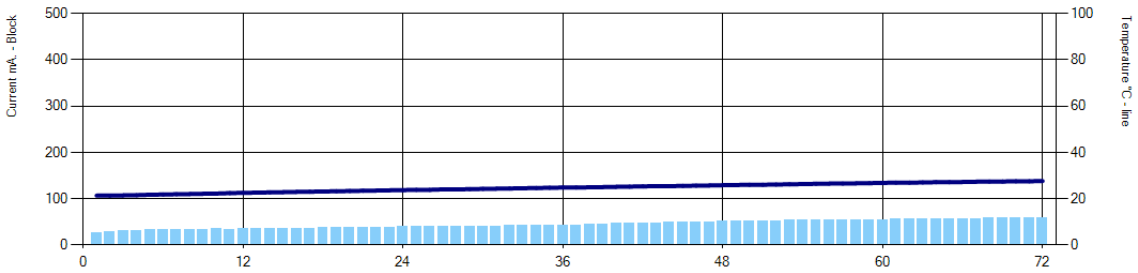

C 10: Sample 100% Z6341 0.42

APPENDIX D: LIMITATIONS AND FUTURE STUDIES

In the elaborated project reported in the thesis, all experiments followed the ASTM Standards. However, additional tests should be done in order to develop the test program.

1. Freeze/thaw test:

In the accelerated study done, 20-25 cycles of freeze/thaw were performed to evaluate the efficiency of the Silane and Transil (organic vs inorganic surface treatment) regarding the resistance of the concrete surface to frost damage in the presence of deicer chemical. More cycles should be performed according to the ASTM Standards – 50 to 100 cycles.

2. Rapid Chloride Penetration Test:

This test has been performed on mortar treated specimens. This test could be eventually performed on reinforced concrete specimens treated with Silane to study the corrosion of the rebars as a function of time and exposure to chloride ions.

3. Abrasion Test:

Consider the gradation of the aggregates at the surface of the specimen and determine the best gradation that suits the Silane application or any other surface treatment.

More samples treated with the same surface treatments should be abraded in order to identify the standard deviation at the end of the test.

4. Lithium penetration:

Since the XRF test was not able to identify the Lithium penetration, other direct/indirect tests should be performed. This element shouldn't go deeper than 2-4mm from the concrete surface. Its concentration can reveal the degree of resistance to abrasion and consequently find the optimum rate of application of the surface treatment as a function of time, load application and degree of damage acceptable for a concrete pavement.